Chapter 4

Experimental and Simulation Study of the Superstructure and Its Components

Jacek Kukulski

Additional information is available at the end of the chapter

http://dx.doi.org/10.5772/61517

Abstract

The issues discussed in this chapter are of interest of both the manufacturers and the experts responsible for condition of the track superstructure. In general, stress in steel elements may affect the energy state, phase changes, and corrosion. It may reduce fatigue strength and cause damage and cracks of the rails. It is one of the causes of accelerated development of standard railhead defects. Proper selection of, e.g., bending process parameters provides uniform distribution and acceptable level of residual stresses in the bent components. Residual stresses that develop during manufacturing process in the railway turnout steel components can change their strength properties. The first part of this chapter presents ultrasonic measurement method and computer simulation that allowed to develop a method to diagnose state and distribution of residual stresses in steel components of the railway turnout (wing rails and switch blades) in the production process. The second part of this chapter includes experimental and simulation studies of superstructure in operational conditions. A track substructure with a crashed stone composite is a solution of reinforced standard track substructure. The results are used to draw conclusions concerning further development and possible modifications of a proposed solution. A significant number of simulation calculations also allow to determine the duration of guaranteed functionality of a reinforced track substructure.

Keywords: Railway turnout, residual stress, ultrasonic measurements, finite-element method, ABAQUS railway track, crashed stone composite

1. Introduction

The development of the railway infrastructure at the turn of the 20th and 21st centuries and the increase in passenger train speed to V_{max} = 300–350 km/h and freight train speed to V_{max} = 140–160 km/h on some routes are the results of railway vehicle design improvement and railway infrastructure optimization.

Track superstructure allowing to reach high speeds and transfer even higher stresses and loads up to 25–30 tonnes per vehicle axle is required to meet very strict strength and durability requirements.

The infrastructure is subject to complex dynamic effects, changing with the increase in load and speed. In the last several decades, standard railway track structure have not change significantly, even though it is subject to studies and improvements aimed at increasing railway traffic safety and limiting operating costs.

The durability of the track superstructure is also affected by the quality of materials used, e.g., steel components used in production of railway turnouts. Steel components of the track superstructure (rails, switch blades) show internal stresses even in the manufacturing process due to process treatment including surface hardening and bending. The treatment introduces additional energy to the material, i.e., stresses, which does not weaken the material, although may affect component operation and result in damage.

2. Review of the literature

Standard railway tracks include a permanent way with the rails and the sleepers on a ballast, operating under load in elasto-plastic state. The ballast is a source of permanent (plastic) deformation. The advanced technological and material solutions allow the operation of the rail bed under operating load in elastic state [1, 2]. Several developed mathematical models of the railway track, its components, and the effect of a vehicle on the track have been detailed in [4, 5].

Nowadays, a finite element method (FEM) is one of the most commonly used methods in addressing complex engineering issues. The method can be used in many fields, to easily create various areas and shapes of complex geometry. Numerical methods have been used in railway track component development for several decades. Extended studies have been performed by the Warsaw University of Technology, the Cracow University of Technology, and other research and development institutes. The studies have included residual stress analysis in steel turnout components, i.e., all rails, including flat-bottom rails.

The aim of the numerical calculations is to determine residual stresses in a rail after relieving and to determine the influence of different parameters on stress size and pattern. The results of numerical calculations have been compared to the results of ultrasonic stress measurements. The studies of international researchers have included modeling the effects observed as a result of rail rolling on roller straighteners. The studies [7] have included rail models and residual stress patterns after rolling simulation and the effect of the rolling process on stress size and pattern. A finite element method, as a basic tool in today's mechanics, has also found its use in railway track and bed development.

As mentioned in various studies, the authors of refs. [8, 12] have presented the results of numerical calculations for created models, as well as the results of measurements performed on testing track sections and in laboratory conditions. The author of this chapter uses FEM for

http://dx.doi.org/10.5772/61517

simulation calculations of static and dynamic loads of the railway track components [13–15]. Standard railway tracks include a permanent way with the rails and the sleepers on a ballast, operating under load in elasto-plastic state. The ballast is a subject to permanent strain resulting in plastic deformation. The advanced technological and material solutions allow the operation of the rail bed under operating load in elastic state [16, 17]. The weakest point of the standard railway track is a compacted crushed stone layer. Several research studies on crashed stone quality, type, and grading as well as on the mechanical compaction methods [18] have been presented. The studies have not given satisfactory results in relation to the reduction of increase in non-uniform plastic strain intensity of the ballast. As a consequence, systematic and frequent repairs are required to eliminate unacceptable geometrical unevenness of a railway track. An energy generated at the wheel/rail interface is transmitted by the rail and rail fixings to the sleepers and via ballast to the rail bed causing an intense vibration field. Kinetic energy increases with the increase in train speed, and as a result, a vibration acceleration of rails, sleepers, ballast, and rail bed increases. It results in considerable tensile stresses within the ballast, affecting internal friction balance and causing ballast to breakup. The ballast subsidence (plastic strain) cannot be avoided, and at the same time it increases with the increase in ballast stresses and vibration acceleration.

Crashed stone ballast layer is subject to tensile stresses. Vibrations in the ballast layer cause acceleration exceeding the acceleration of gravity g, further reducing ballast resistance to tensile stresses. Crashed stone ballast layer at sleeper and ballast interface at operational loads is in a spatial compressive stress state. The principal stress tensor can be described as $\sigma_1 > \sigma_2 > \sigma_3 > 0$. It means that the crashed stone ballast is in a tri-axial compression state thus creating the best conditions for ballast operation. The most adverse conditions can be observed when the ballast is subject to pulsating and variable tensile stresses. Further analysis shows that the tensile stresses are most likely to occur near the rail fixing point, i.e., point of wheel-ballast-crashed stone ballast load transmission and in the areas from the side of the ballast face. Top ballast layer in those areas requires protection against factors that may cause deconsolidation. Stress analysis in the track subgrade shows that the tensile stresses decay in the track subgrade at the depth of 60 ÷ 80 cm.

3. Residual stress

Residual stresses are considered stresses counteracting each other inside the component, which is not affected by any external loads. Internal loads are a measure of elastic strain energy stored in a specific body area and are additional component loads. Assuming a plane internal strain state of the stresses on the component surface (rail), normal and shear stresses can be defined [20], see Figure 1.

Components of plane stress state:

- σ_x, σ_y, σ_z
- τ_{xy}, $\tau_{xz} = \tau_{yz} = 0$

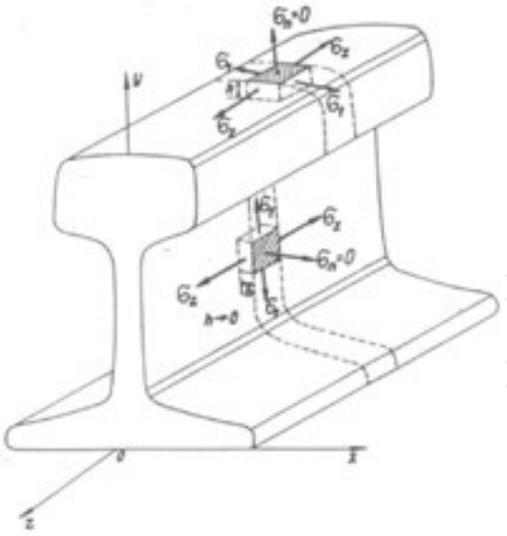

Figure 1. Components of plane stress state on rail surface [21].

The stresses on the rail surface are defined by normal stresses and tangential stresses σ_n, σ_t.

Each component at the rail surface without load meets the following condition:

$$\sigma_n = 0 \; i \sigma_t = 0$$

For those conditions, the relation between strain and stress is as follows:

$$\varepsilon_z = \frac{1}{E}\left(\sigma_z - \nu\sigma_t\right) \tag{1}$$

$$\varepsilon_t = \frac{1}{E}\left(\sigma_t - \nu\sigma_z\right) \tag{2}$$

$$\tau_{tn} = 0 \tag{3}$$

Residual stresses σ_z and σ_t can be determined based on Equations (4) and (5):

$$\sigma_z = \frac{E}{1-\nu^2}\left(\varepsilon_z + \nu\varepsilon_t\right) \tag{4}$$

$$\sigma_t = \frac{E}{1-\nu^2}\left(\varepsilon_t + \nu\varepsilon_z\right) \tag{5}$$

http://dx.doi.org/10.5772/61517

where σ_t tangential stress, σ_z is the normal stress, ε_t is the tangential strain, ε_z is the horizontal residual strain, and ν is the Poisson ratio.

3.1. The phenomenon of residual stresses

The residual stress arises in the case of heterogeneous plastic deformation caused by

- bending and cold rolling
- thermal stresses
- heterogeneous phase transitions

For steel railway superstructure components, occurrence and change in residual stresses are due to thermal stresses and plastic strain resulting from bending and cold rolling.

Thermal stresses are a result of non-uniform phase transitions due to thermal treatment, including surface hardening, used for shaping the steel turnout components. The treatment aims to increase hardness of the surface layer of a wing rail or a switch blade.

The effect of generating residual stresses in this case is more complex compared to heterogeneous cold strain. It is affected by a temperature gradient and resulting thermal stresses, including phase change processes, recrystallization, relaxation, and dependence of material properties on temperature. For steel railway superstructure components, occurrence and change in residual stresses are due to thermal stresses and plastic strain resulting from bending and cold rolling. Thermal stresses are a result of non-uniform phase transitions due to thermal treatment, including surface hardening, used for shaping the steel junction components. The treatment aims to increase hardness of the surface layer of a wing rail or a switch blade.

Residual stresses in hardened steel components are due to a martensitic transformation at lower temperatures, where an overcooled austenite transforms into a martensite—a phase with lower density or other structures depending on requirements and thermal processes (hardening). The transformation of overcooled austenite can be conveniently analyzed based on an austenite decomposition graph, also called isothermal transformation diagrams (or time–temperature–transformation (TTT) diagrams). If the thermal and textural stresses overlap, as is the case with steel hardening, the direction and the size of residual stresses after the temperature is even in the component cross section are determined by the offset in the transformation initiation stage in the surface area and in the core in relation to the moment the thermal stress sign reverses. In other words, the textural stresses tend to increase or reduce the thermal stresses depending on the cross section, cooling rate, and steel hardening capacity [20].

The depth of hardened layer also affects the distribution of residual stresses after hardening. Non-uniform plastic strain or temperature gradient will thus result in residual stresses. The rails and switch blades after rolling and quenching do not often meet the requirements on straightness and require straightening using special roller straighteners. Maintaining the required rail straightness is particularly important at high travel speeds. The process introduces significant longitudinal residual stresses. For rails straightened on the roller straighteners, as a result of variable strain of surfaces in contact and not in contact with the rollers, 150–300

MPa residual stresses over the running surface of a head and at the bottom of a rail foot, and –100 to 200 MPa compressive stresses at a rail web are recorded.

3.2. Experimental studies of residual stresses

Residual stress values can be obtained by experiments and theoretical analysis. The methods of theoretical determination of residual stresses involve solving complex thermal, elastic, and plastic relations. It is a complex solution, due to lack of accurate data on actual loads exerted on an object. The theoretical analysis of residual stresses is bound up with the elastic theory and elastic properties, plastic flow and material hardening, heat transfer, phase transitions, thermal expansion, structure, and thickness of surface layer. The complexity of processes that occur in the material during process treatment means that the results of the theoretical analysis are based on simplified models and cannot be used to evaluate the residual stress state even in components with straight geometry and require use of the experimental method. The residual stresses have been the topic of interest for the researchers and scientist for several decades. Thus, various methods and techniques for measuring the residual stresses were developed. Generally, residual stress measurement methods in steel components can be divided into two categories: destructive and non-destructive methods. Destructive methods do not allow to determine the quality of tested objects without damage, whereas non-destructive methods allow multiple tests on the same object.

Ultrasonic method used by the author to determine the residual stresses is based on the relation between ultrasonic wave velocity and stress. Ultrasonic wave velocity is determined with an accuracy of a fraction of a meter per second to measure the residual stresses with required precision. To measure the absolute values, the effects of temperature and non-uniform distribution of elastic properties and material texture on the wave velocity must be allowed for. A relatively easy and simple method is the ultrasonic measurement with DEBRO-35 instrument. The method uses electro-acoustic effects, i.e., a relation between stress and velocity or time the ultrasonic wave requires to cover a specific distance (at the surface zone). The residual stresses are measured using a special measuring head system that records longitudinal and lateral surface waves (Figure 2).

The meter measurement circuits allow for the effect of rail temperature change to the velocity of wave propagation. The head system features temperature sensor, providing information required for automatic compensation of a velocity of wave propagation at different temperatures.

The advantage of the method is the ability to perform non-destructive testing in field conditions, compact and easy-to-use system, and the ability to display the measurement results. In addition, the preparation of tested section surface does not require time-consuming operations.

3.2.1. The experimental wing rail and switch blade tests

Experimental rail section tests were performed on components subject to rolling, surface hardening and bending into wing rails used in the railway turnouts.

http://dx.doi.org/10.5772/61517

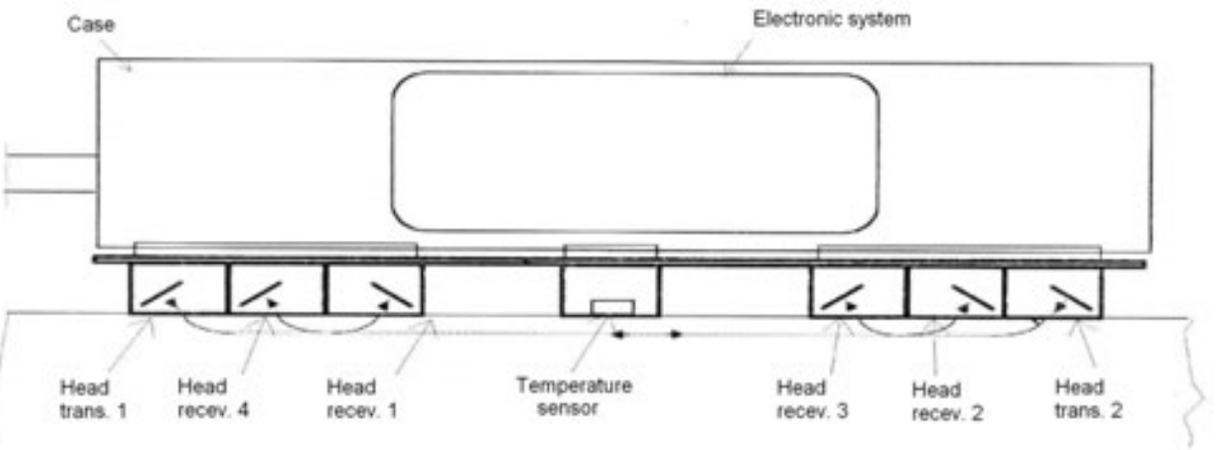

Figure 2. Special measuring head system in ultrasonic instrument DEBRO-35.

3.2.1.1 The transverse bending of the switch blades and wing rails

3.2.1.1. The transverse bending of the switch blades and wing rails

The specimens were bent in the steelworks manufacturing railway turnouts (former Koltram S.A., Zawadzkie), involved three- and four-point bending. Figures 3–6 show the method of section bending including the point of support and force causing the strain as well as cross sections used.

The specimens were bent in the steelworks manufacturing railway turnouts (former Koltram S.A., Zawadzkie), involved three- and four-point bending. Figures 3–6 show the method of section bending including the point of support and force causing the strain as well as cross sections used.

.

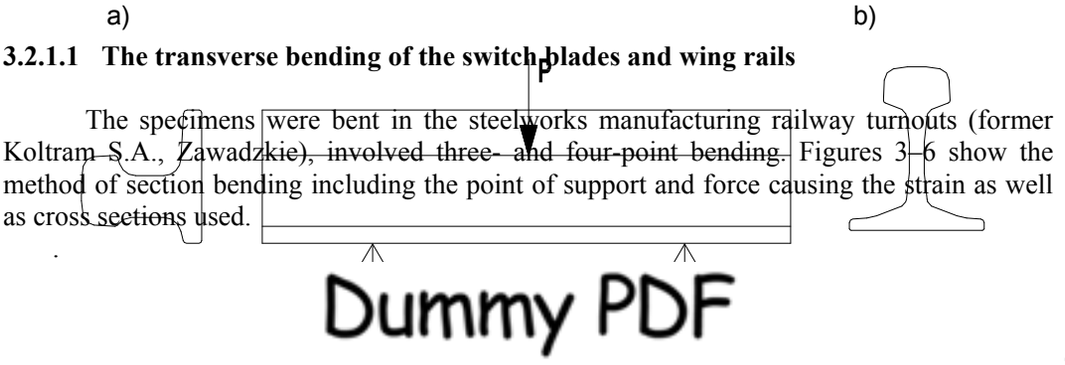

3.2.1.1 The transverse bending of the switch blades and wing rails

The specimens were bent in the steelworks manufacturing railway turnouts (former Koltram S.A., Zawadzkie), involved three- and four-point bending. Figures 3–6 show the method of section bending including the point of support and force causing the strain as well as cross sections used.

.

Figure 3. Three-point transverse bending of the switch blade I60 (a) and wing rail (b) sections.

Figure 3. Three-point transverse bending of the switch blade I60 (a) and wing rail (b) sections.

Figure 3. Three-point transverse bending of the switch blade I60 (a) and wing rail (b) sections.

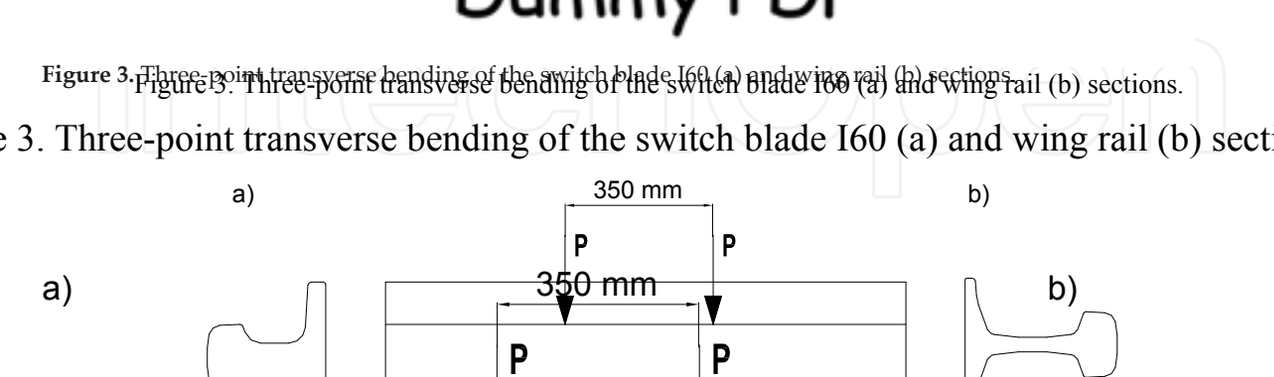

Figure 4. Four-point transverse bending of the switch blade I60 (a) and wing rail (b) sections.

Figure 4. Four-point transverse bending of the switch blade I60 (a) and wing rail (b) sections.

Figure 4. Four-point tı ʒ rail (b) sections.

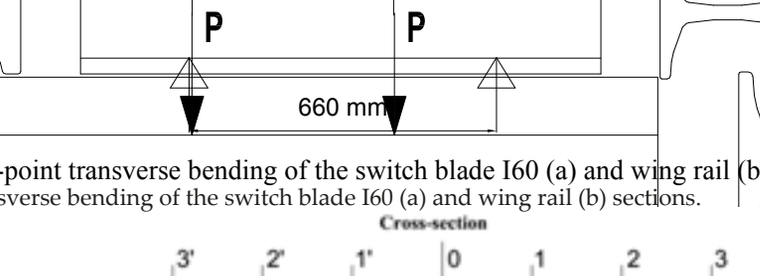

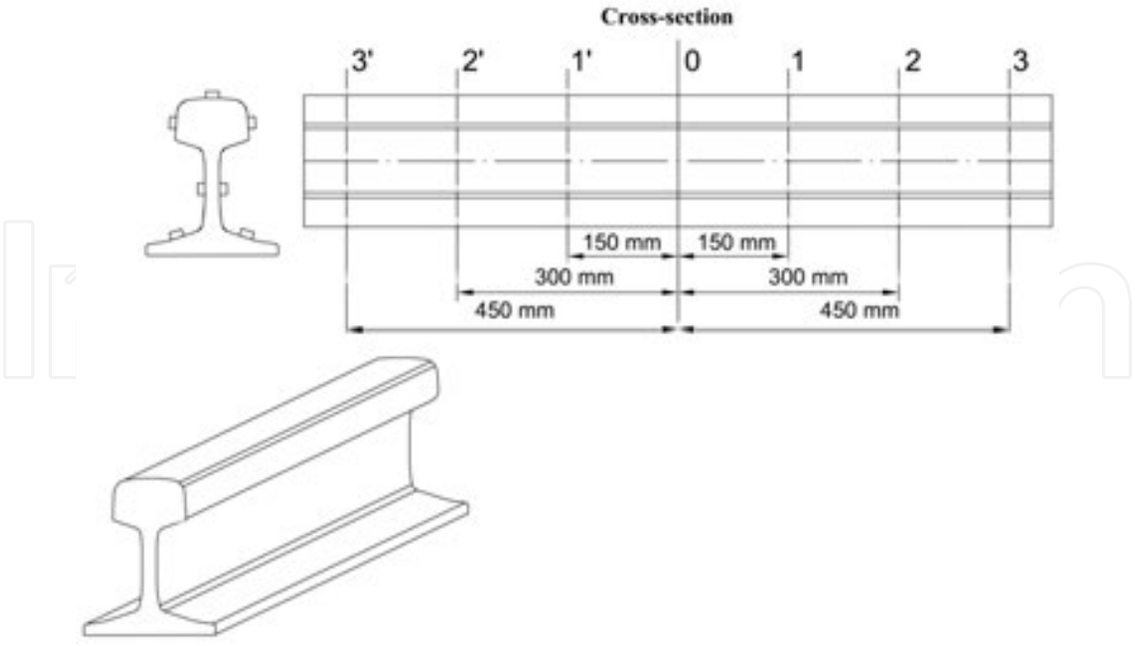

Figure 5. Measurement places at the circumference of rail UIC 60.

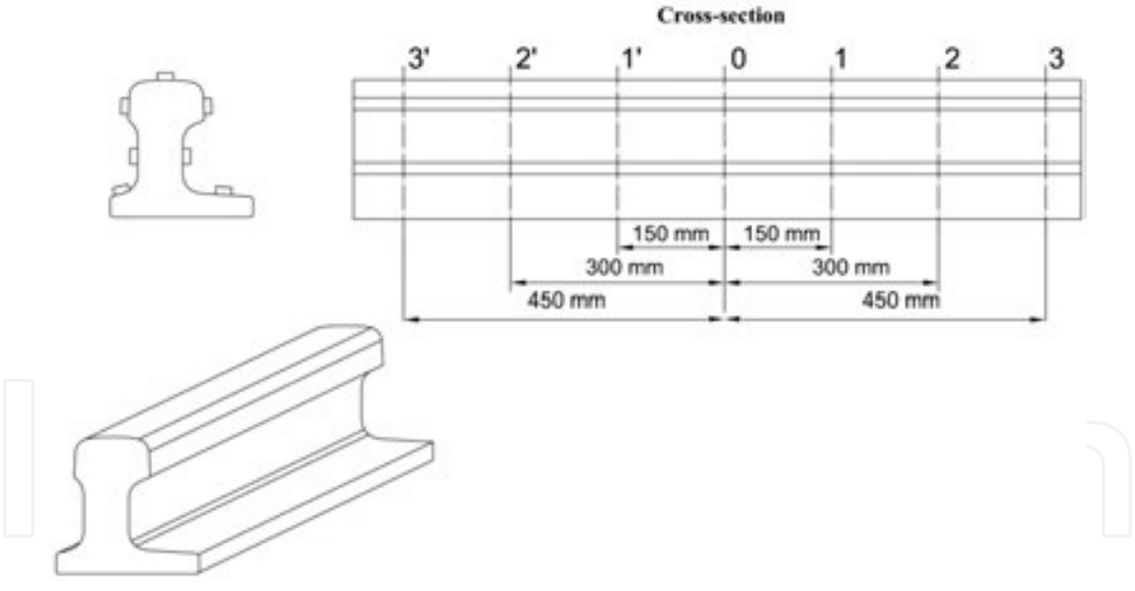

Figure 6. Measurement places at the circumference of rail I60.

3.2.1.2. Results of residual stress measurement—bending process

The diagrams (Figures 7–10) show example of longitudinal stress changes at the circumference of rail and switch blades after bending processes of selected sections. A horizontal axis represents a distance from the centre of a head rolling surface (measured at the rail and switch point surface), and vertical axis represents the longitudinal component of a residual stress.

The diagrams (Figures 7–10) show example of longitudinal stress changes at the circumference of rail and switch blades after bending processes of selected sections. A horizontal axis represents a distance from the centre of a head rolling surface (measured at the rail and switch point surface), and vertical axis represents the longitudinal component of a residual stress.

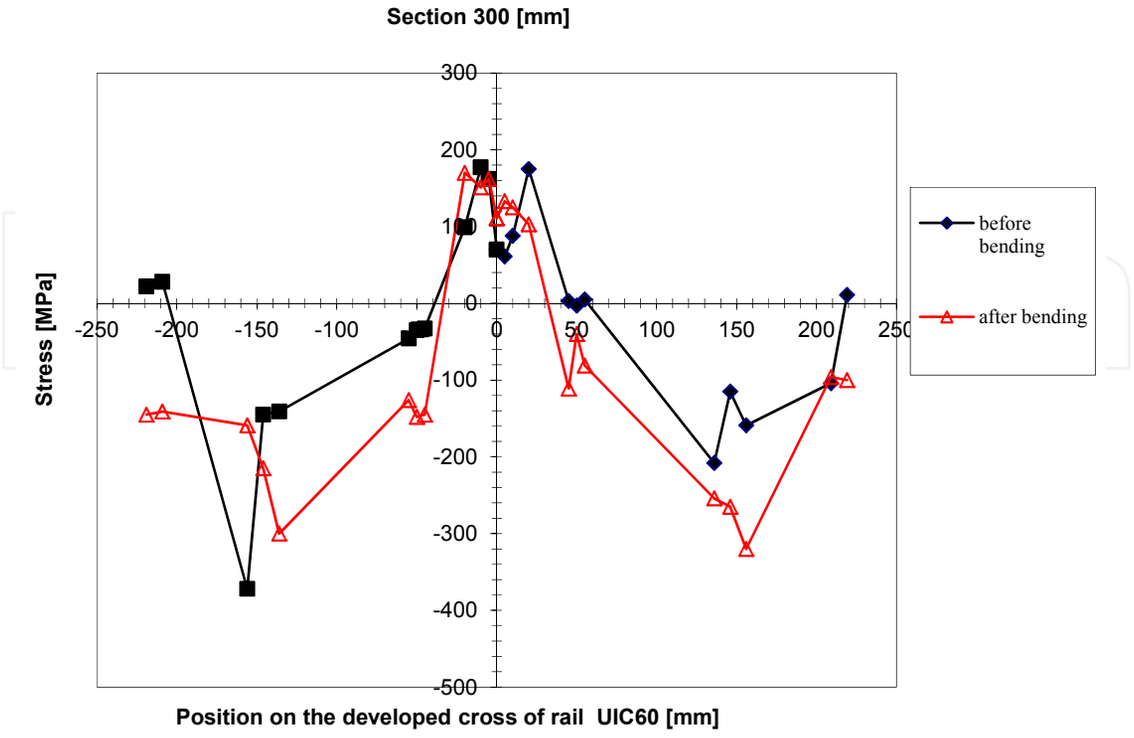

Figure 7. Longitudinal stress changes at the circumference of rail UIC 60 before and after three point bending processes (section 300 mm).

Figure 7. Longitudinal stress changes at the circumference of rail UIC 60 before and after three point bending processes (section 300 mm).

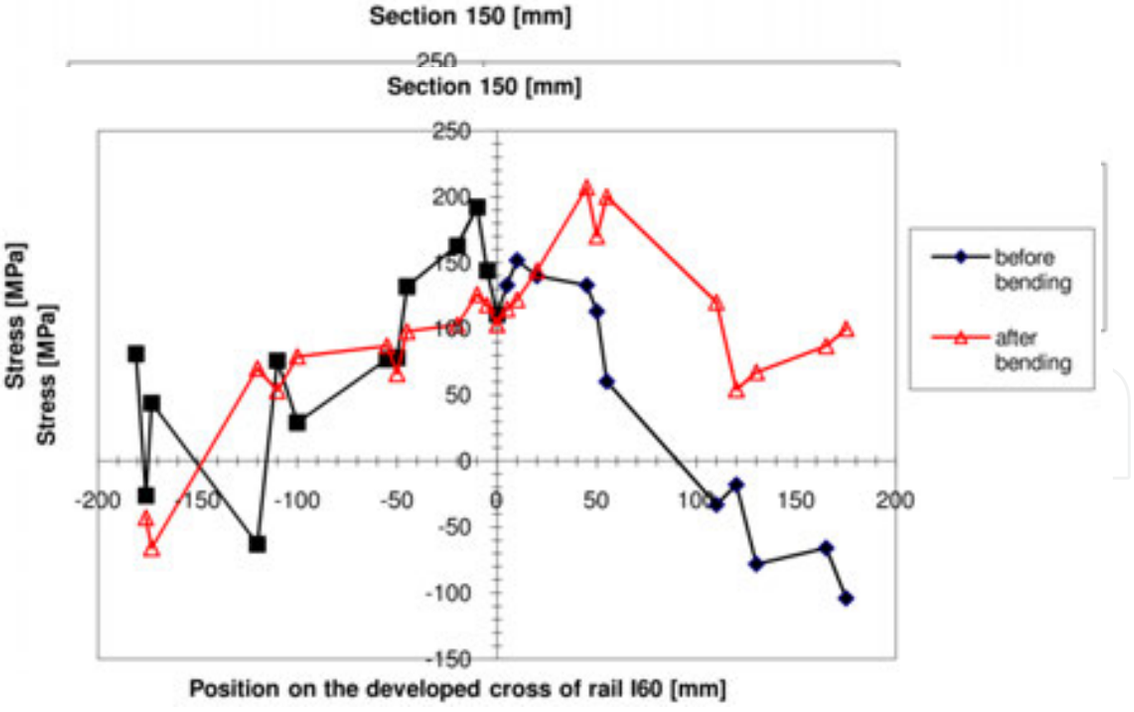

Figure 8. Longitudinal stress changes at the circumference of rail I60 before and after three point bending processes (section 150 mm).

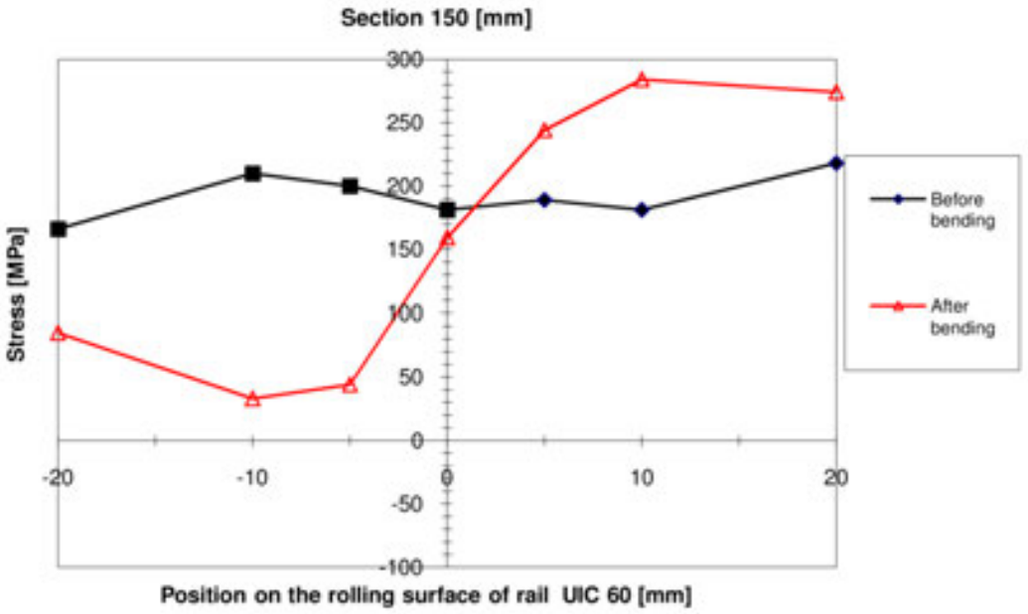

Figure 9. Longitudinal stress changes on the top surface of rail UIC 60 before and after four point bending process (section 150 mm).

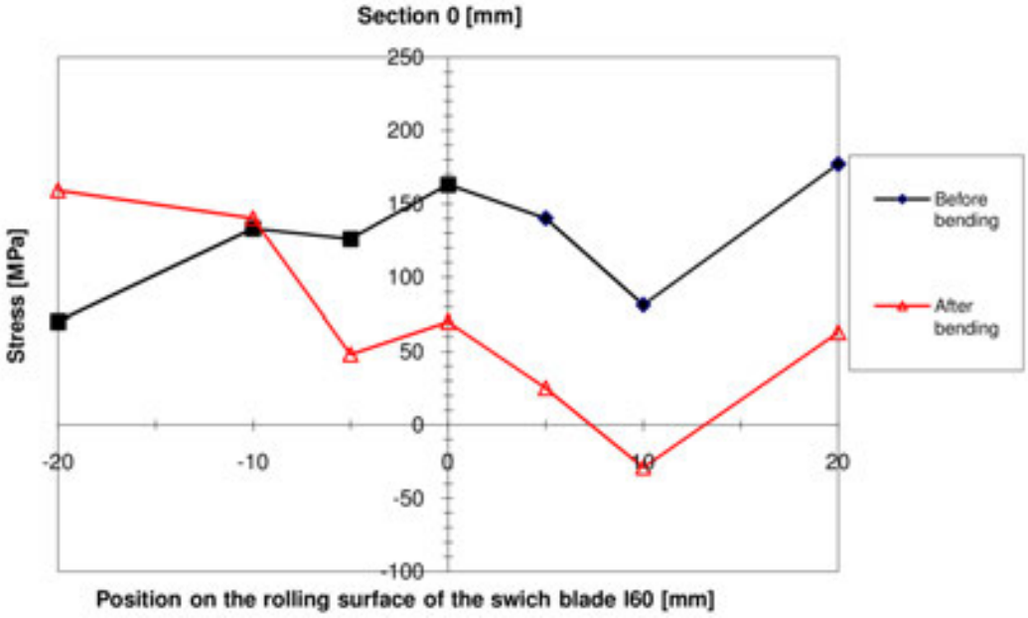

Figure 10. Longitudinal stress changes on the top surface of rail I60 before and after four point bending process (section 0 mm).

The results of measurements for residual stresses obtained with ultrasonic testing show after the bending tests that in case of four-point bending the distribution and size of residual stresses is more favorable and uniform compared to the three-point bending case. Numerous research works and service observations show that from practical point of view, the most dangerous

http://dx.doi.org/10.5772/61517

proves to be the maximum tensile stress σ_{max}, which may accelerate the development of cracking process and cause permanent deformation of the steel components.

3.2.2. Surface hardening switch blades and wing rails

After the bending process, the switch blades and wing rails are subject to a pearlitizing process in the course of hardening the rolling surfaces. As a result of flame heating of a rolling surface to the depth of up to 20 mm, and subsequent cooling with water mist and compressed air, a fine pearlitic structure with specified hardness is obtained. The heat stream from flame heating is generated by the special nozzles (burners) installed on the surface hardening station. The temperature of heated running surface shall not exceed 673K (400°C). Figures 11 and 12 show hardening zones of steel components.

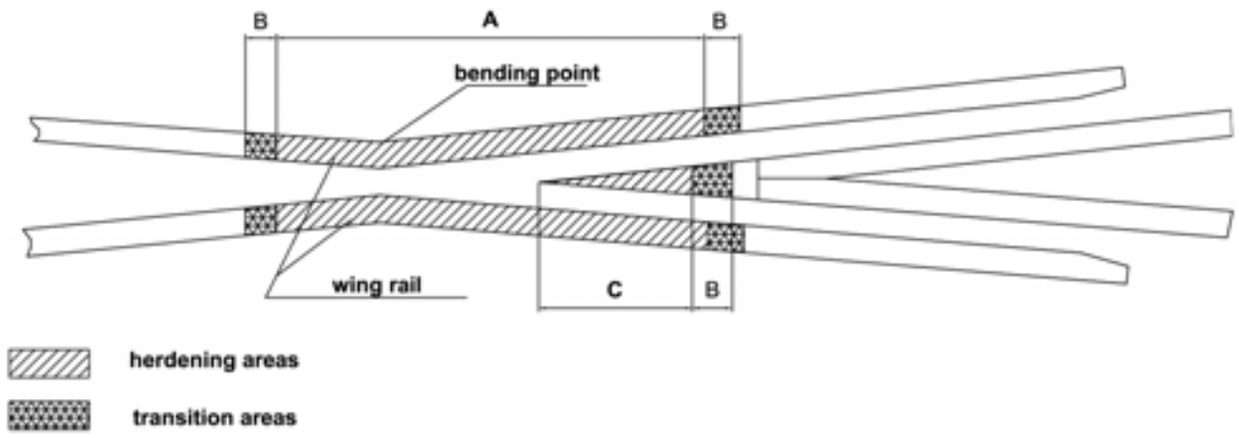

Figure 11. Heat treatment areas of the wing rail UIC 60 and actual frog point.

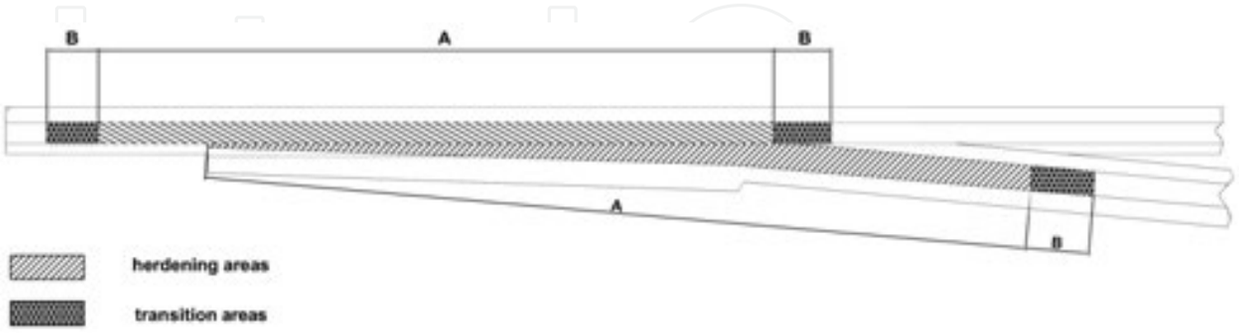

Figure 12. Heat treatment areas of the switch blade I60.

The diagrams presented further on (Figures 13 and 14) show examples of longitudinal stress changes at the circumference of rail and switch blade after hardening and bending processes for the selected sections.

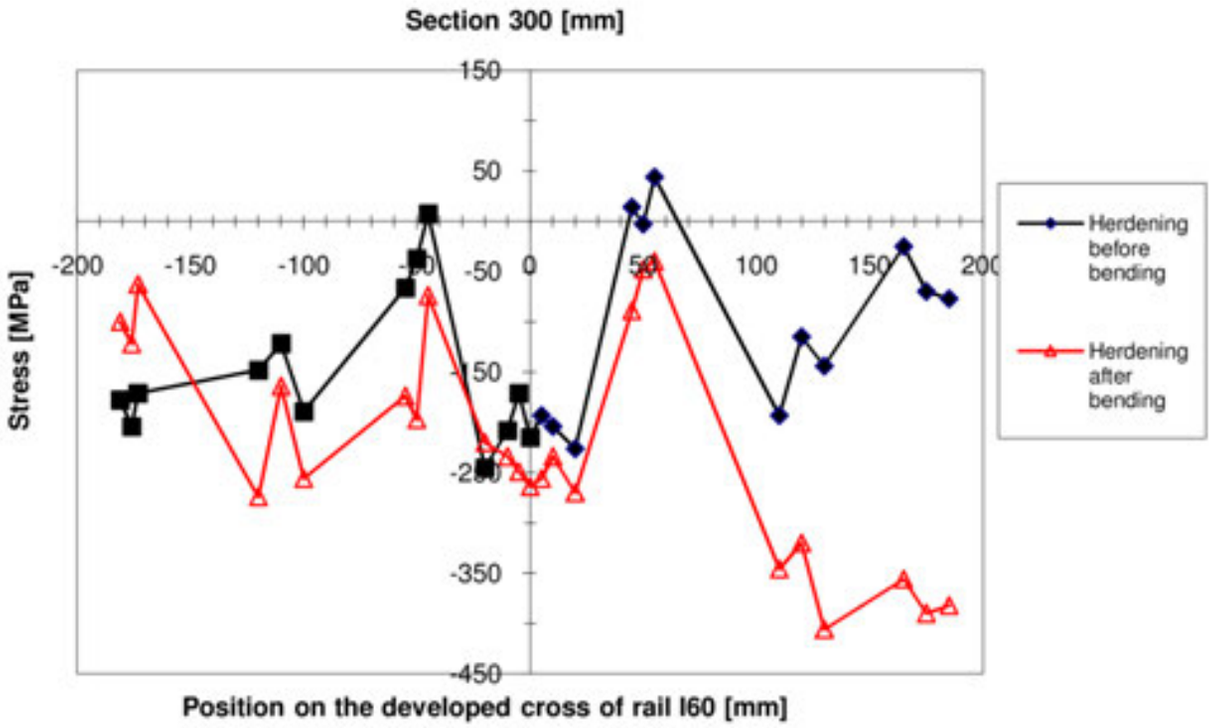

Figure 13. Longitudinal stress changes at the circumference of rail I60 after heat treatment and after bending processes (section 300 mm).

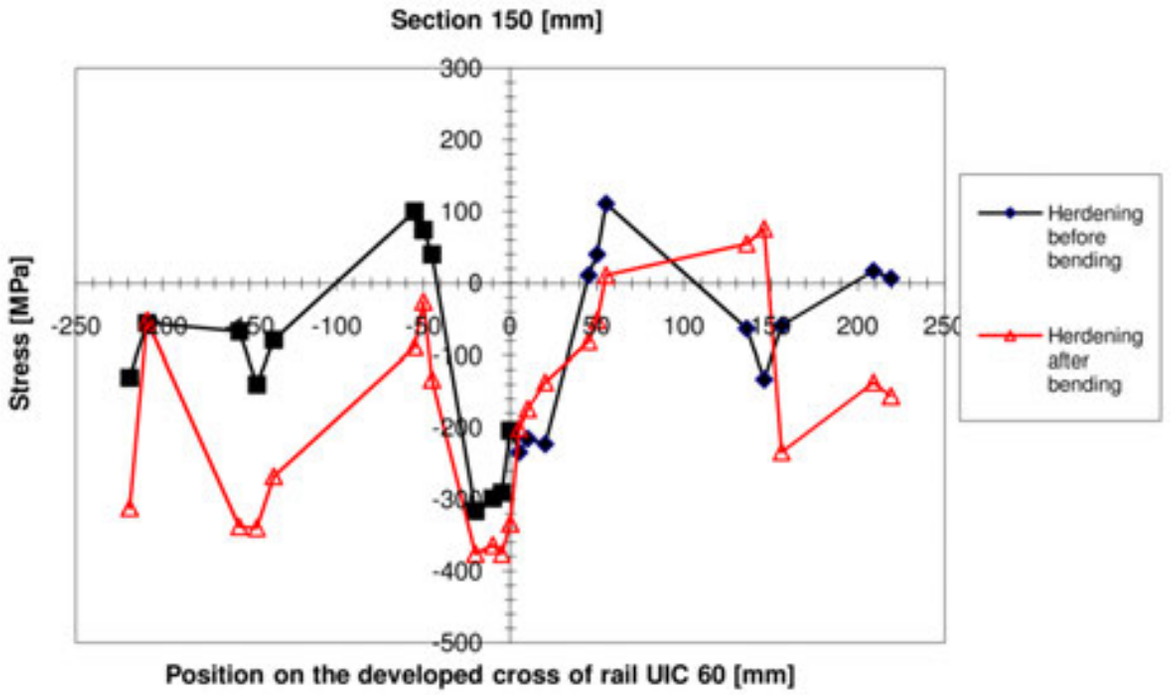

Figure 14. Longitudinal stress changes at the circumference of rail UIC 60 after heat treatment and after bending processes (section 150 mm).

http://dx.doi.org/10.5772/61517

3.3. FEM simulation studies

The subject of the numerical analysis in this paper is simulation of three- and four-point bending, rolling, and surface hardening processes of the section samples of UIC 60 rail and I60 switch blade. The analysis concerns strains and stresses generated in the course of the above-mentioned technological operations. The main purpose of the numerical calculations is to determine residual stresses in the rail after the relief that happens after bending and/or hardening process. It is also to define the influence of different test parameters on the size and distribution of stresses. Structure models and numerical calculations were made using the ABAQUS—a software with an extensive capabilities of non-linear analysis of physical issues, including mechanics of the deformable solids.

3.3.1. The material of the model

Figure 15 shows experimental curve–stress σ vs. strain ε for a single axis steel tensile test (black line). Young's modulus E = 210.000 MPa and Poisson ratio ν = 0.3 were used for calculations. Point A is defined with a non-proportional elongation proof stress σ_A = 629.7 MPa. Point A in the approximation curve divides the elastic state from the plastic–elastic state with hardening. Point B is selected at the curvilinear hardening section for stress σ_B = 900.0 MPa. Point C is determined by maximum stress achieved during test, i.e., temporary strength R_m = 1069.0 MPa. Besides, stress and strain values for the approximation curves (red line) were determined for each temperatures represented in Figure 15.

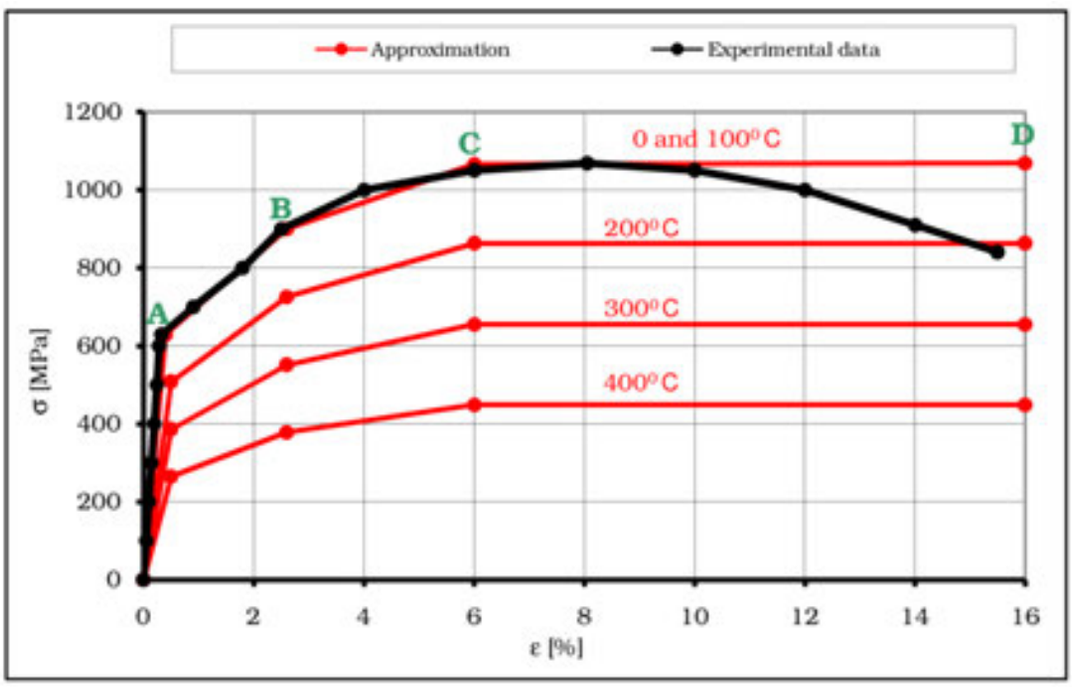

Figure 15. Experimental material curve and its approximation $\sigma - \varepsilon$ depending on the heating temperature.

3.3.2. Load and boundary conditions

The way of support and the load application used in the experiment were replaced by ideal boundary conditions in the numerical model. The calculation process was divided into two steps. The first corresponding to the loaded state condition, and the second corresponding to the condition realized state. The way of support was defined by reduction of the specific degrees of freedom in the nodes, which correspond to the experiment are present in the support sections (Figure 16). During simulation of the surface hardening, the rail may show longitudinal displacement as a result of material expansion due to rolling surface heating.

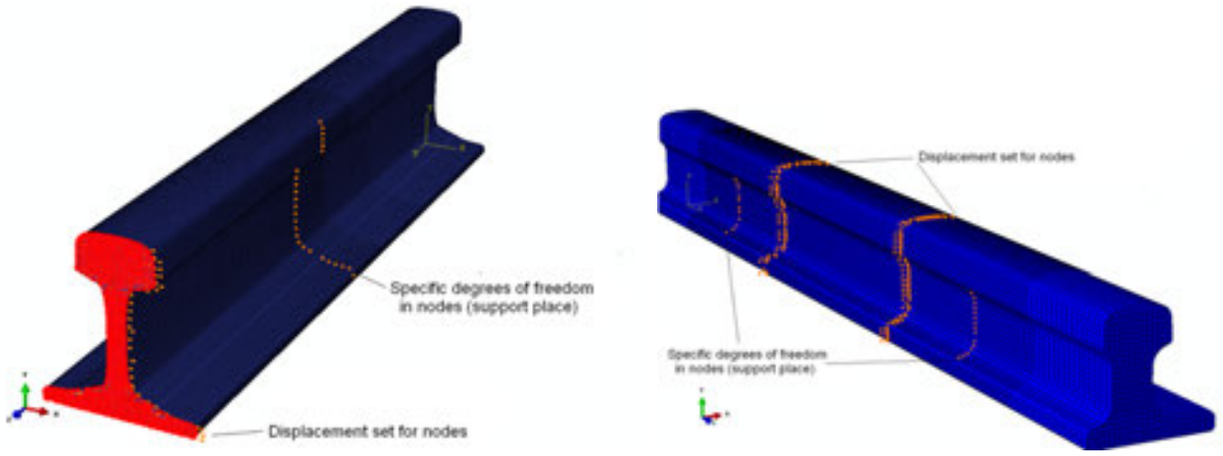

(a) (b)

Figure 16. Finite element models of UIC 60 (a) and I60 (b) rail with boundary conditions and loading—three and four point transverse bending.

Figure 16. Finite element models of UIC 60 (a) and I60 (b) rail with boundary conditions and loading—three and four point transverse bending.

During simulation of the rail section rolling, the roller force on the rail and the roller speed are set. The load was increased gradually (incrementally), and the system of equation was solved to determine the increment in strain, stress, and displacement. The rail was supported by two adjacent rollers at specific centers (Figure 17).

During simulation of the rail section rolling, the roller force on the rail and the roller speed are set. The load was increased gradually (incrementally), and the system of equation was solved to determine the increment in strain, stress, and displacement. The rail was supported by two adjacent rollers at specific centers (Figure 17).

3.3.3. Results of numerical analysis

Several simulation calculations covering different variants of section bending, surface hardening, and rolling process were performed. Figures 18–21 show the results of computer simulation for UIC 60 rail and I60 switch blade models. The figures show contours of the of reduced stress σ^{HM} and residual stress σ_{11} after relief.

Numerical calculation results shown in Figures 18–21 provided a number of interesting data in addition to the experimental tests. Allocation of extreme stresses around the periphery of analyzed objects may be determined based on the results obtained.

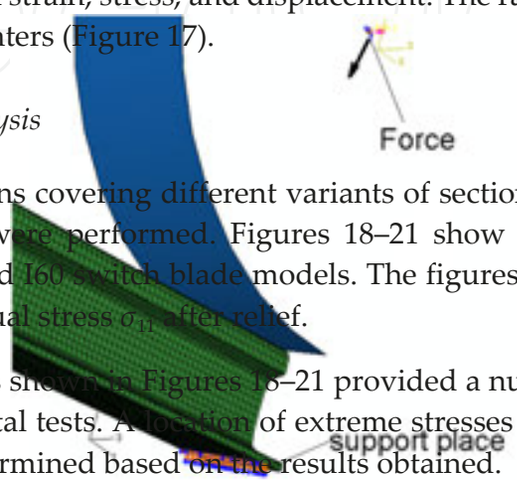

Figure 17. Finite element models of UIC 60 rail with boundary conditions and loading—the rolling process.

3.3.3 Results of numerical analysis

Several simulation calculations covering different variants of section bending, surface hardening, and rolling process were performed. Figures 18–21 show the results of computer

http://dx.doi.org/10.5772/61517

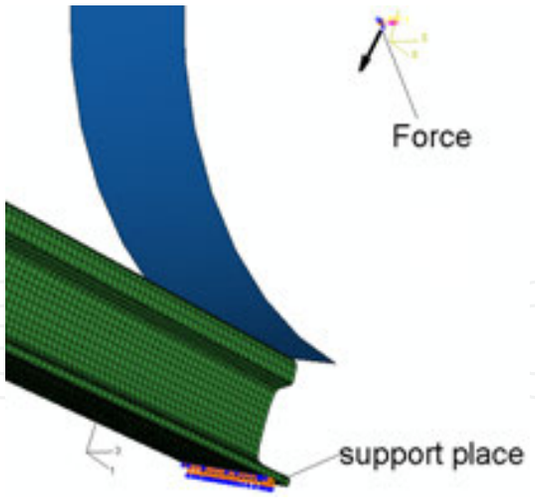

Figure 17. Finite element models of UIC 60 rail with boundary conditions and loading—the rolling process.

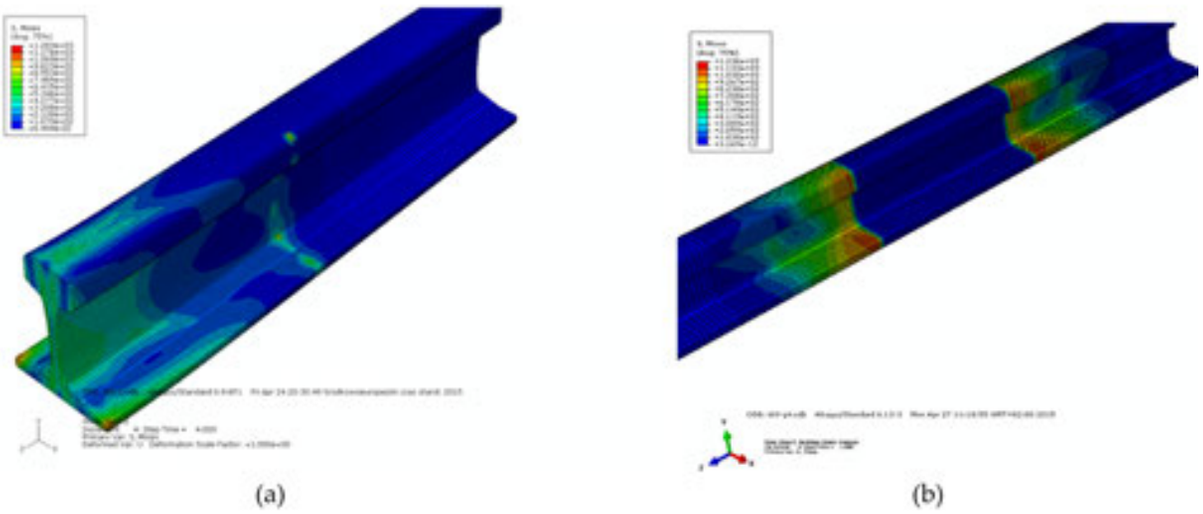

Figure 18. Contours of reduced stress σ^{HM} of the rail UIC 60 (a) and I60 (b) switch blade section after three (a) and four (b) point bending.

3.4. The evaluation of residual stresses

Use of ultrasonic measurement method (DEBRO-35 measuring instrument) and computer simulation allowed to develop a method to diagnose state and distribution of residual stresses in steel components of the railway turnout (wing rails and switch blades) in the production process [15]. The method involves summation of residual stresses measured prior to treatment (bending, hardening) and stresses during simulation. The method allows to assess the level and distribution of residual stresses achieved using different bending or hardening processes. The example results of diagnosing residual stresses are shown in Figures 22 and 23.

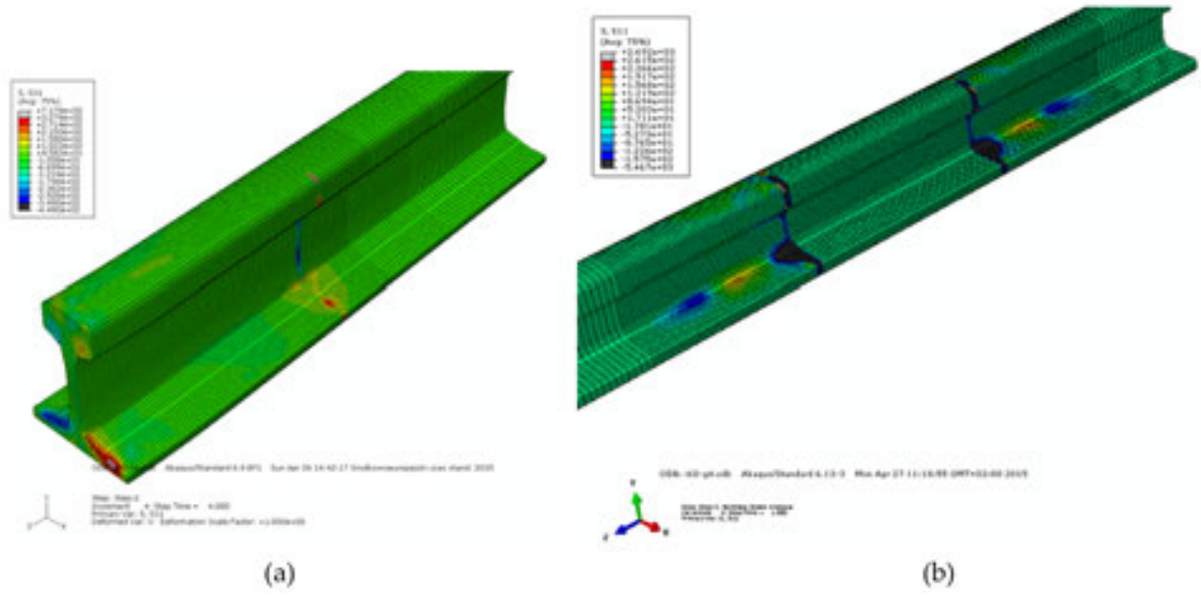

Figure 19. Contours of residual stress σ_{11} of the rail UIC 60 and I60 switch blade section after three (a) and four (b) point bending.

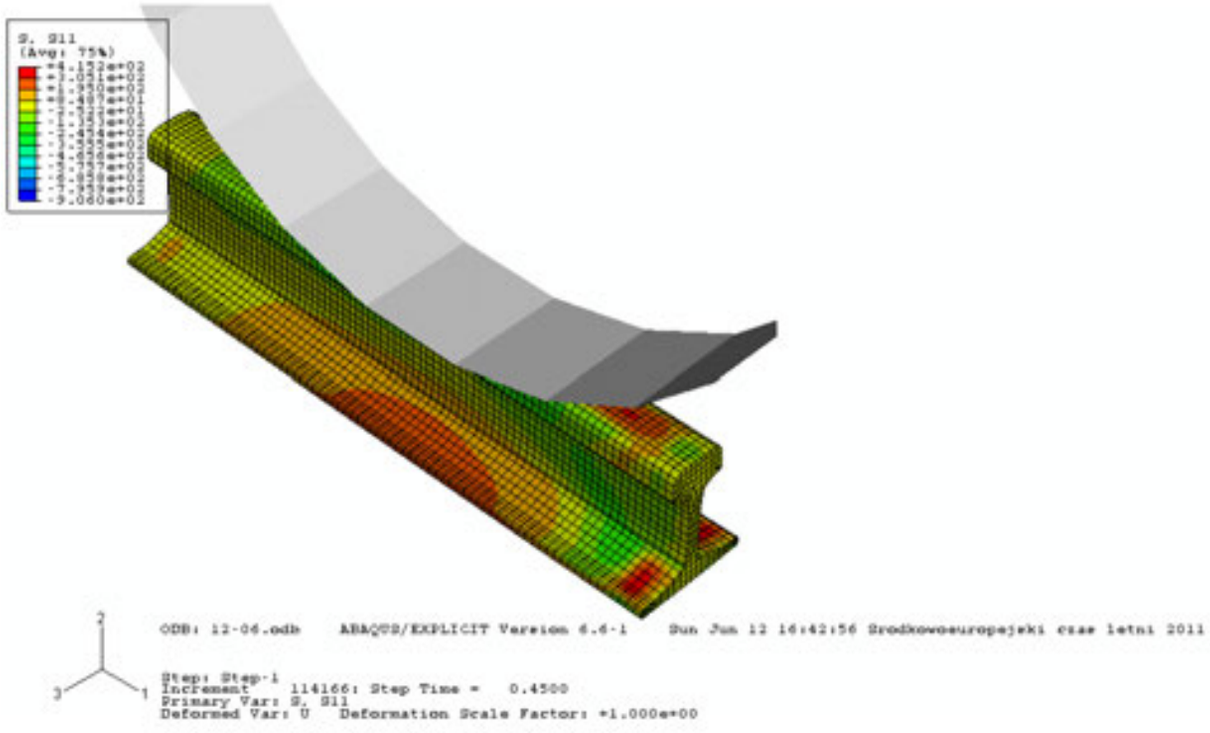

Figure 20. Contours of residual stress σ_{11} of rail UIC 60 after rolling process [14].

http://dx.doi.org/10.5772/61517

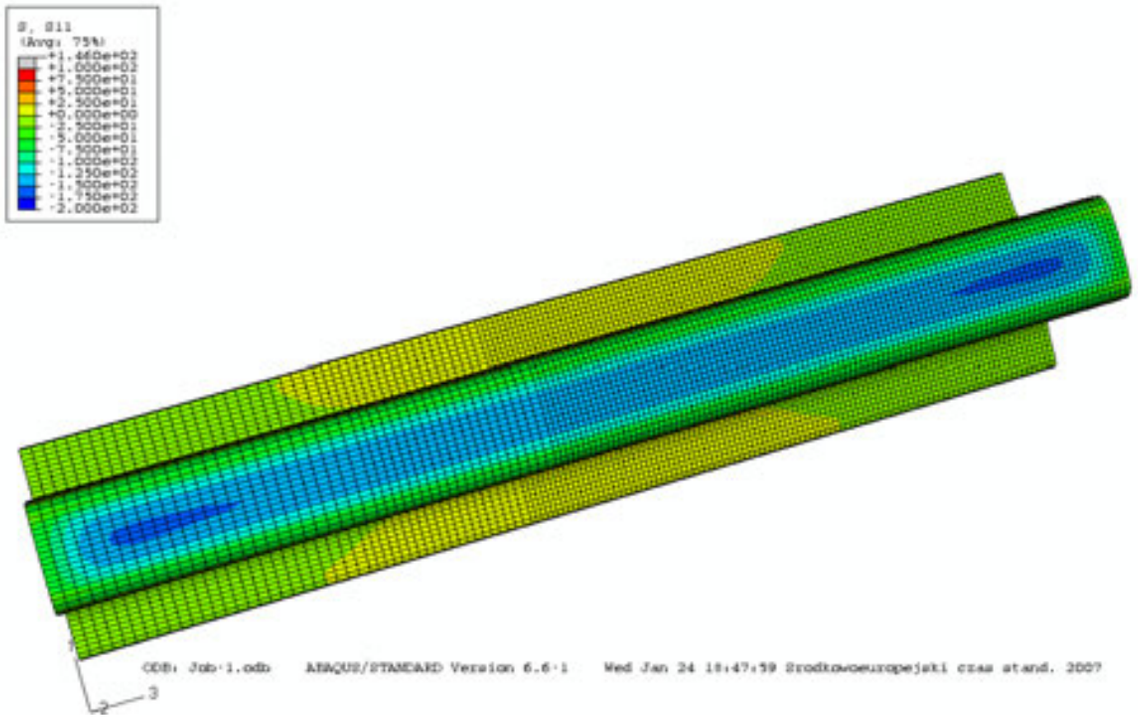

Figure 21. Contours of residual stress σ_{11} on the head of rail UIC 60 after heat treatment.

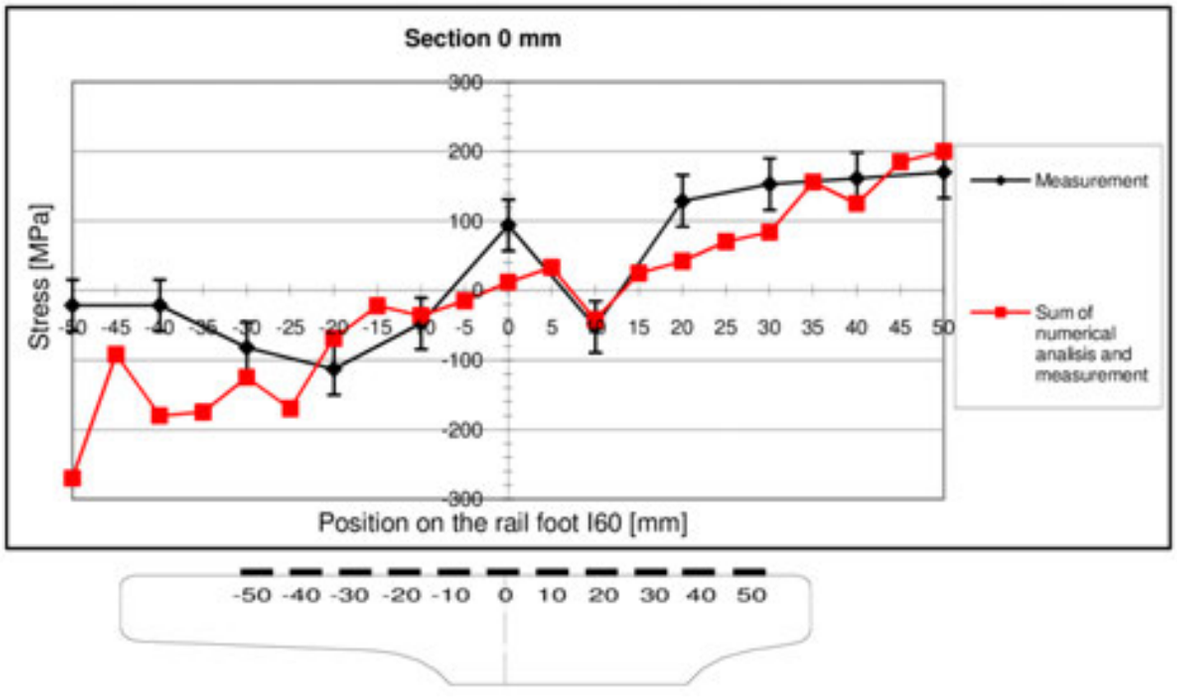

Figure 22. Comparison of measurement results of residual stress after cold bending (rail foot I60) with results summarizing stresses from the numerical analysis and measurements before bending (section 0 mm).

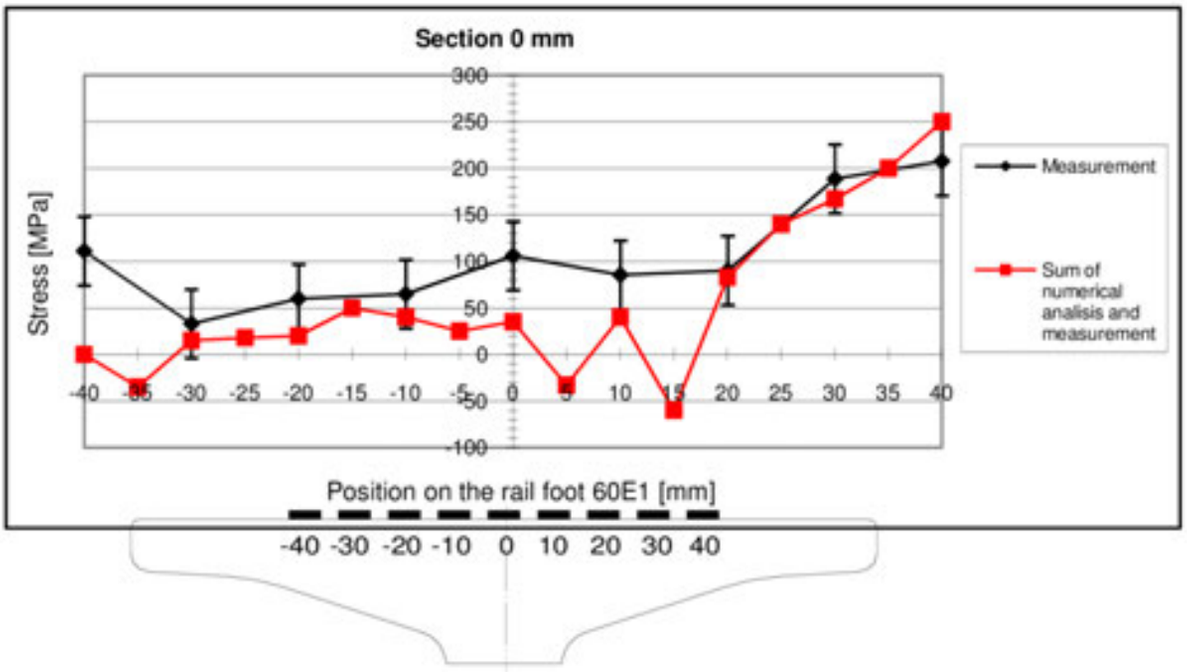

Figure 23. Comparison of measurement results of residual stress after cold bending (rail foot UIC60) with results summarizing stresses from the numerical analysis and measurements before bending (section 0 mm).

4. Operational research of superstructure

4.1. Experimental studies

Using crashed stone composite in the form of a ballast bed reinforced with geogrids and local chemical stabilization of crashed stone is one of the possible answers to the question how to improve the ballast resistance to deformation. The solution has been developed by the Division of Transport Infrastructure of the Warsaw University of Technology Faculty of the Transport (by T. Basiewicz, K. Towpik, A. Gołaszewski) [22]. The proposed crashed stone composite comprises a layer of crashed stone reinforced with a geogrid and stabilized with a polyurethane resin. The track superstructure with a crashed stone composite ensures a complex mechanical and chemical resistance of the ballast to deconsolidation. Mechanical resistance is ensured by reinforcement with at least two geogrids. The first geogrid covers the area of ballast contact with a subgrade. After the first crashed stone layer is laid and compacted, the second geogrid is placed. After the second layer of crashed stone is laid (to obtain a required thickness of ballast under the sleeper, as per standard requirements), it is compacted and supplemented to the standard shape of a stockpile. In the final stage with a dynamic surface stabilization, the structure is chemically stabilized with a special polyurethane resin by injection. Figure 24 shows the layer of ballast reinforced with the geogrid and the resin.

The key purpose of the track geometry measurements for the track structures section with crashed stone composite was to evaluate the deformability of the track vs. the adjacent

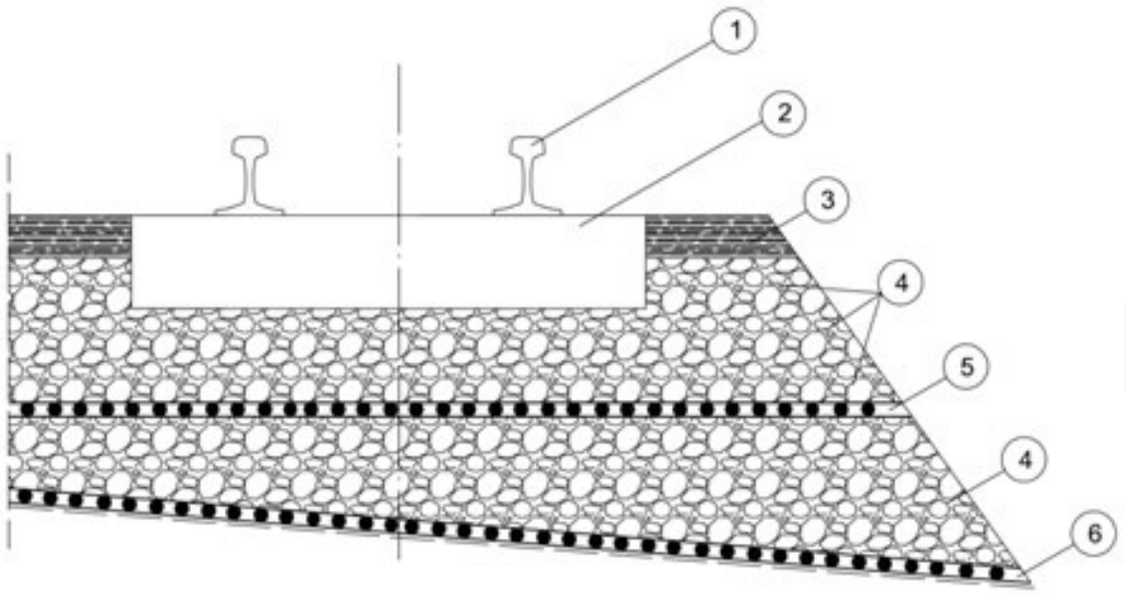

Figure 24. Track structures with crashed stone composite [13]. 1—rail UIC 60, 2—sleeper, 3—crashed stone layer with resin, 4—crashed stone layer, 5—top reinforcement (geogrid, geosynthetic), 6—bottom reinforcement (geogrid, geosynthetic)

comparative track sections. Results of measurements, of the EM 120 measuring motor car, made during 17 trips between 2008 and 2013 were used in the evaluation of track geometry deformability. The traffic load in that period was approximately 18 Tg. Changes in the quality index result and changes in the standard deviation for vertical and horizontal track irregularities provide an indirect description of ballast bed deformation.

The values of the quality index "J" were computed as follows

$$J = \frac{S_z + S_y + S_w + 0.5S_e}{3.5} \tag{6}$$

where S_z is the standard deviation for vertical irregularities, S_y is the standard deviation for horizontal irregularities, S_w is the standard deviation for track twist, and S_e is the standard deviation for track gauge.

The studies [22] present complete test results covering the entire test period. Figures 25 and 26 show selected test results for track superstructure with crashed stone.

4.2. Simulation studies

The simulations complement the experimental tests performed at the section of "CMK" (railway central trunk line—an element of the Polish railways network). Figure 27 shows a schematic railway track model used in simulation calculations, allowing for the rigidity and attenuation of each railway superstructure component.

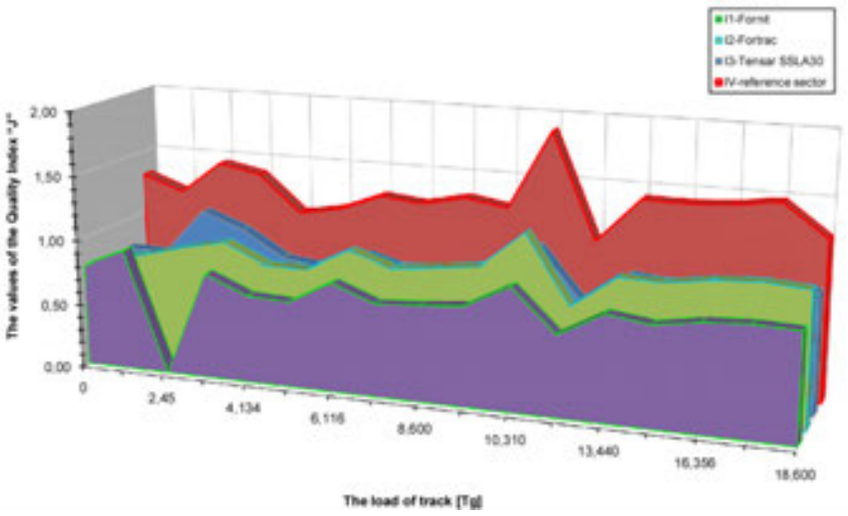

Figure 25. Values of the quality index "J" for different sections of existing subgrade (I1—section No.1 with geogrid; I2—section No.1 with geosynthetic; and I3—section No.2 with geogrid) vs. reference sector IV.

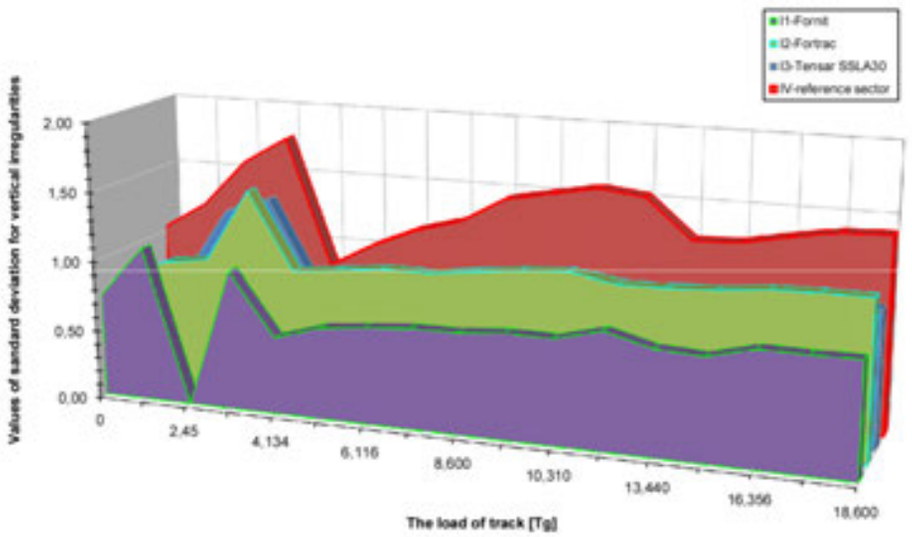

Figure 26. Values of standard deviation for vertical irregularities for different sections of existing subgrade (I1—section No.1 with geogrid; I2—section No.1 with geosynthetic; and I3—section No.2 with geogrid) vs. reference sector IV.

The motion of the system may be expressed by the following differential equations:

$$EI\frac{\partial^4 z_r}{\partial x^4} + m_s\frac{\partial^2 z_r}{\partial t^2} + c_{ps}\frac{\partial z_r}{\partial t} + k_{ps}z_r - k_{ps}z_s - c_{ps}\frac{\partial z_s}{\partial t} = P(t)\delta(x), \tag{7}$$

$$m_s\ddot{z}_s + c_s\frac{\partial z_s}{\partial t} + k_s z_s = k_{ps}(z_r - z_s) + c_{ps}\left(\frac{\partial z_s}{\partial t} - \dot{z}_s\right), \tag{8}$$

http://dx.doi.org/10.5772/61517

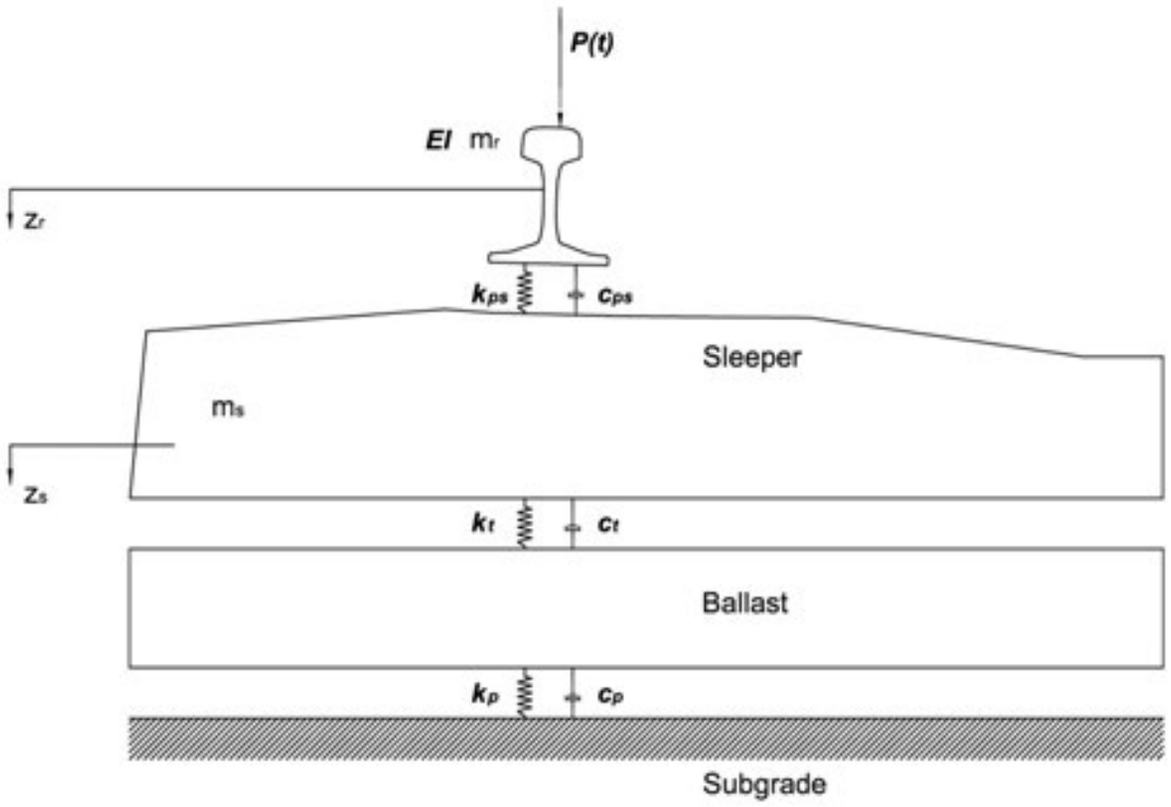

Figure 27. The schematic railway track model used in simulation calculations: $P(t)$—concentrated force; m—mass of elements; EI—bending stiffness of rail; c—damping; k—stiffness.

4.2.1. Model geometry— Finite element grid railway track

Structure models and numerical calculations were made using the ABAQUS—a software. A geometry of a numerical model is defined as a grid of nodes indicating position and size of finite elements. Simplified numerical models of the superstructure were developed, including a single sleeper or three sleepers buried in the ballast.

Due to the complex shape of modeled structures, apart from cuboids with six walls, additional three-dimensional components were also included, solids with a triangular base (with five walls). Square components are considered the most relevant for the description of the issues with bending as a prevailing treatment to better describe stress concentration and allow better approximation of curved shapes with lower number of elements. Figure 28 shows FE railway track models.

For simulation purposes, the interfaces between each of structure components were determined since the development of a complete model grid with the same degree of detail is not feasible. The grids for various components may vary in size. The interface is a surface connecting two adjacent grid segments with various grid densities to maintain the model continuity (Figure 29). It enables a proper distribution of load on adjacent grids to maintain the 3D model homogeneity.

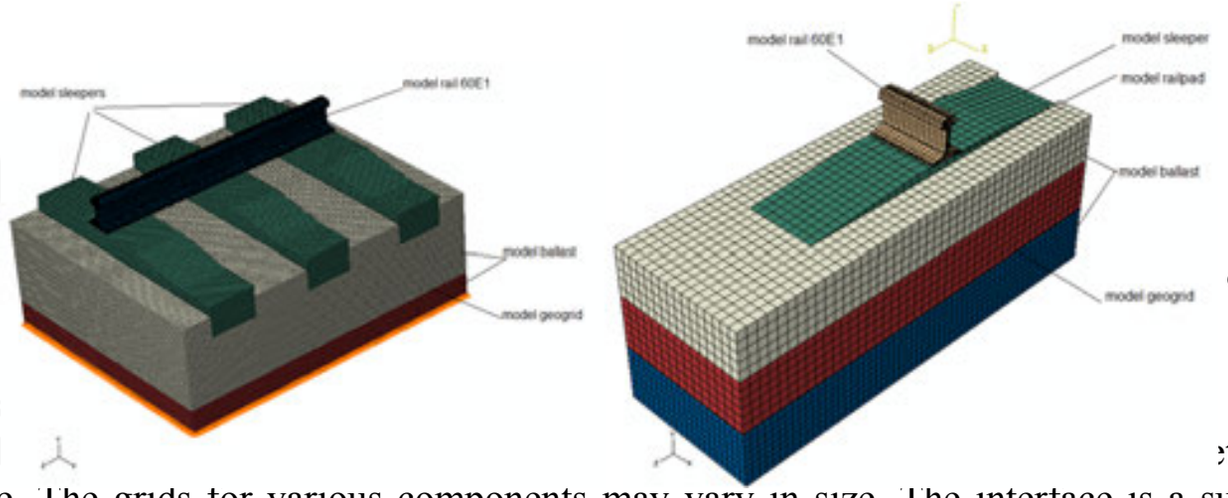

Figure 28. FE railway models of the reinforced surface for (a) three sleepers and (b) one sleeper.

For simul were determined tail is not feasible. The grids for various components may vary in size. The interface is a surface connecting two adjacent grid segments with various grid densities to maintain the model continuity (Figure 29). It enables a proper distribution of load on adjacent grids to maintain the 3D model homogeneity.

For simulation purposes, the interfaces between each of structure components were determined since the development of a complete model grid with the same degree of detail is not feasible. The grids for various components may vary in size. The interface is a surface connecting two adjacent grid segments with various grid densities to maintain the model continuity (Figure 29). It enables a proper distribution of load on adjacent grids to maintain the 3D model homogeneity.

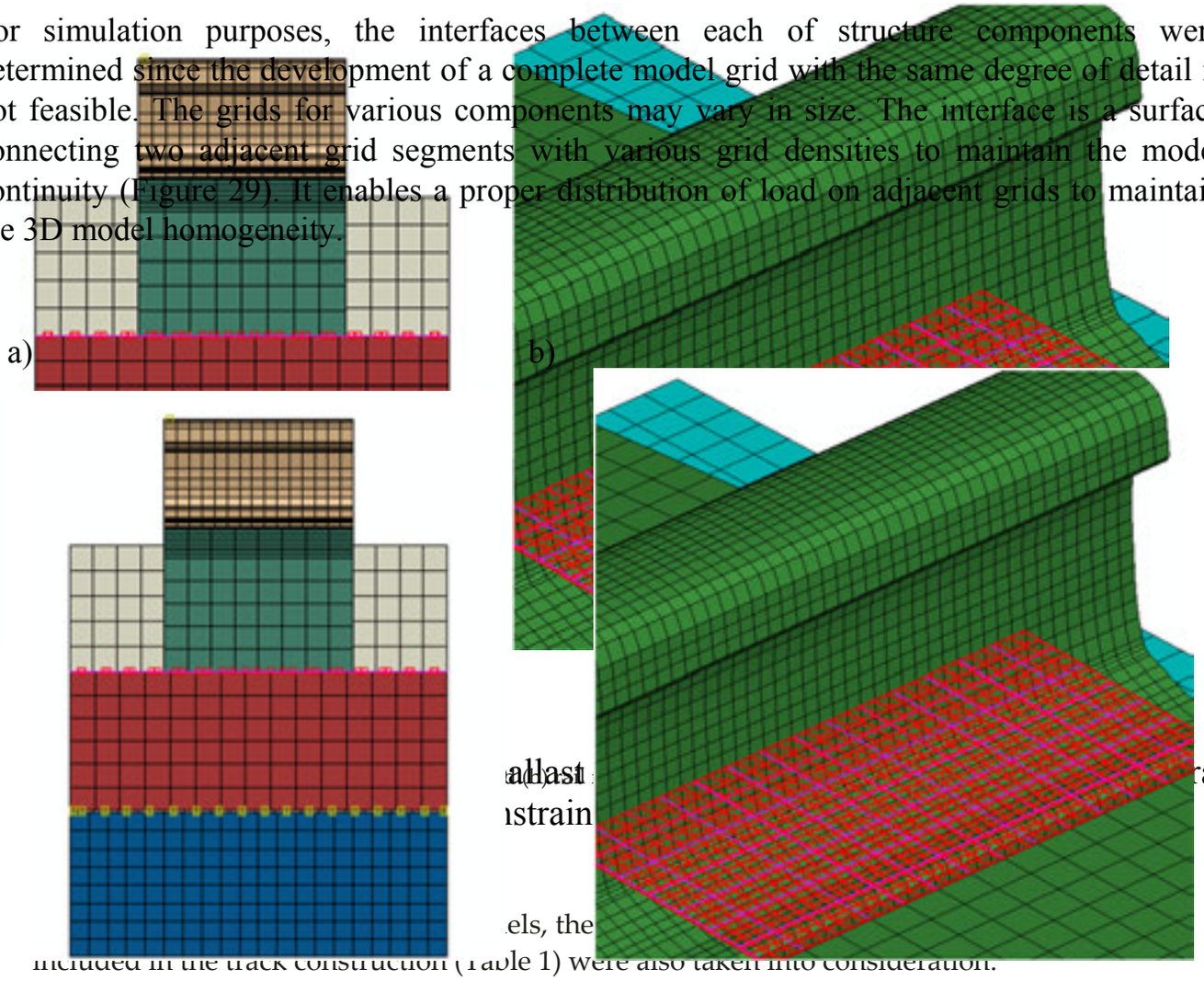

Figure allast ral nstrain

els, the included in the track construction (Table 1) were also taken into consideration.

Figure 29. The interfaces for (a) sleeper/ballast and (b) rail foot/sleeper interface (unilateral constraints) [23].

4.2.2 Material model

In studies on the built simulation models, the parameters of stiffness and damping

http://dx.doi.org/10.5772/61517

Notation	Parameter	Value	Unit
E_r	Elastic modulus of rail	210,000	MPa
k_{ps}	Rail pad stiffness	239	MN/m
c_{ps}	Rail pads damping	30	kNs/m
ρ_b	Ballast density	54	kg/m^3
ρ_r	Rail density	7,850	kg/m^3
E_b	Elastic modulus of ballast	150	MPa
νr	Poisson ratio of rail	0.30	-
νb	Poisson ratio of ballast	0.35	-
νs	Poisson ratio of sleeper	0.30	-
c_p	Ballast damping	250	kNs/m
k_p	Ballast stiffness	110	MN/m
ρ_s	Sleeper density	2,400	kg/m^3
E_s	Elastic modulus of sleeper	70,000	MPa
Eg	Elastic modulus of geogrid	2,200	MPa
νg	Poisson ratio of geogrid	0.5	-
ρ_g	Geogrid density	0.00132	kg/m^3

Table 1. 1The parameters of stiffness and damping elements in the track construction model

4.2.3. Model load and support conditions

Means of support used in the course of testing were substituted with ideal boundary conditions in the numerical model. A static and dynamic cylinder thrust of the cylinder on the rail and the speed of cylinder rotation simulating the vehicle speed were set. The load was increased gradually (incrementally), and the system of equation was solved to determine the increment in strain, stress, and displacement. Support conditions are defined by a specific loss of degree of freedom, preventing from displacement in specific directions (Figure 30).

4.2.4. Results of simulation calculation

The selected results of numerical calculations, obtained using 3D models of a reinforced railway track in different arrangements, are shown in diagrams as Huber–Misess reduced stress contours and strain maps. The Huber–Misess hypothesis of the largest shear stress and the shear strain energy hypothesis are used in the calculation of structures and machine parts with elastic–plastic materials. Figures 31 and 32 show numerical calculation results.

Means of support used in the course of testing were substituted with ideal boundary conditions in the numerical model. A static and dynamic cylinder thrust of the cylinder on the rail and the speed of cylinder rotation simulating the vehicle speed were set. The load was increased gradually (incrementally), and the system of equation was solved to determine the increment in strain, stress, and displacement. Support conditions are defined by a specific loss of degree of freedom, preventing from displacement in specific directions (Figure 30).

Means of support used in the course of testing were substituted with ideal boundary conditions in the numerical model. A static and dynamic cylinder thrust of the cylinder on the rail and the speed of cylinder rotation simulating the vehicle speed were set. The load was increased gradually (incrementally), and the system of equation was solved to determine the increment in strain, stress, and displacement. Support conditions are defined by a specific loss of degree of freedom, preventing from displacement in specific directions (Figure 30).

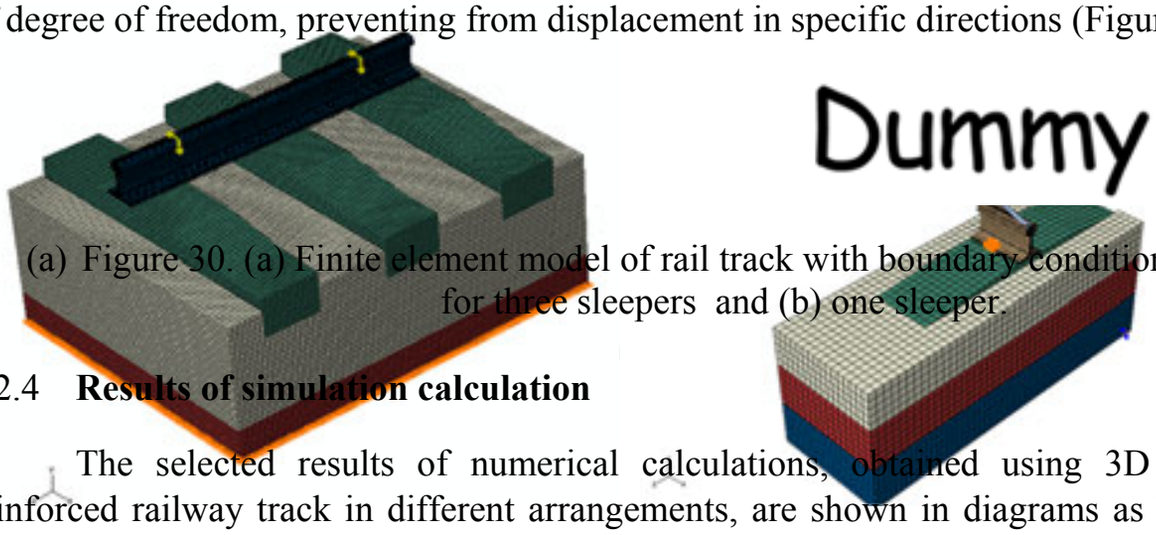

(a) (b)

Figure 30. (a) Finite element model of rail track with boundary conditions and loading for three sleepers and (b) one sleeper.

(a) Figure 30. (a) Finite element model of rail track with boundary conditions and loading for three sleepers and (b) one sleeper.

4.2.4 Results of simulation calculation

The selected results of numerical calculations, obtained using 3D models of a reinforced railway track in different arrangements, are shown in diagrams as Huber–Misess reduced stress contours and strain maps. The Huber–Misess hypothesis of the largest shear stress and the shear strain energy hypothesis are used in the calculation of structures and machine parts with elastic-plastic materials. Figures 31 and 32 show numerical calculation results.

4.2.4 Results of simulation calculation

The selected results of numerical

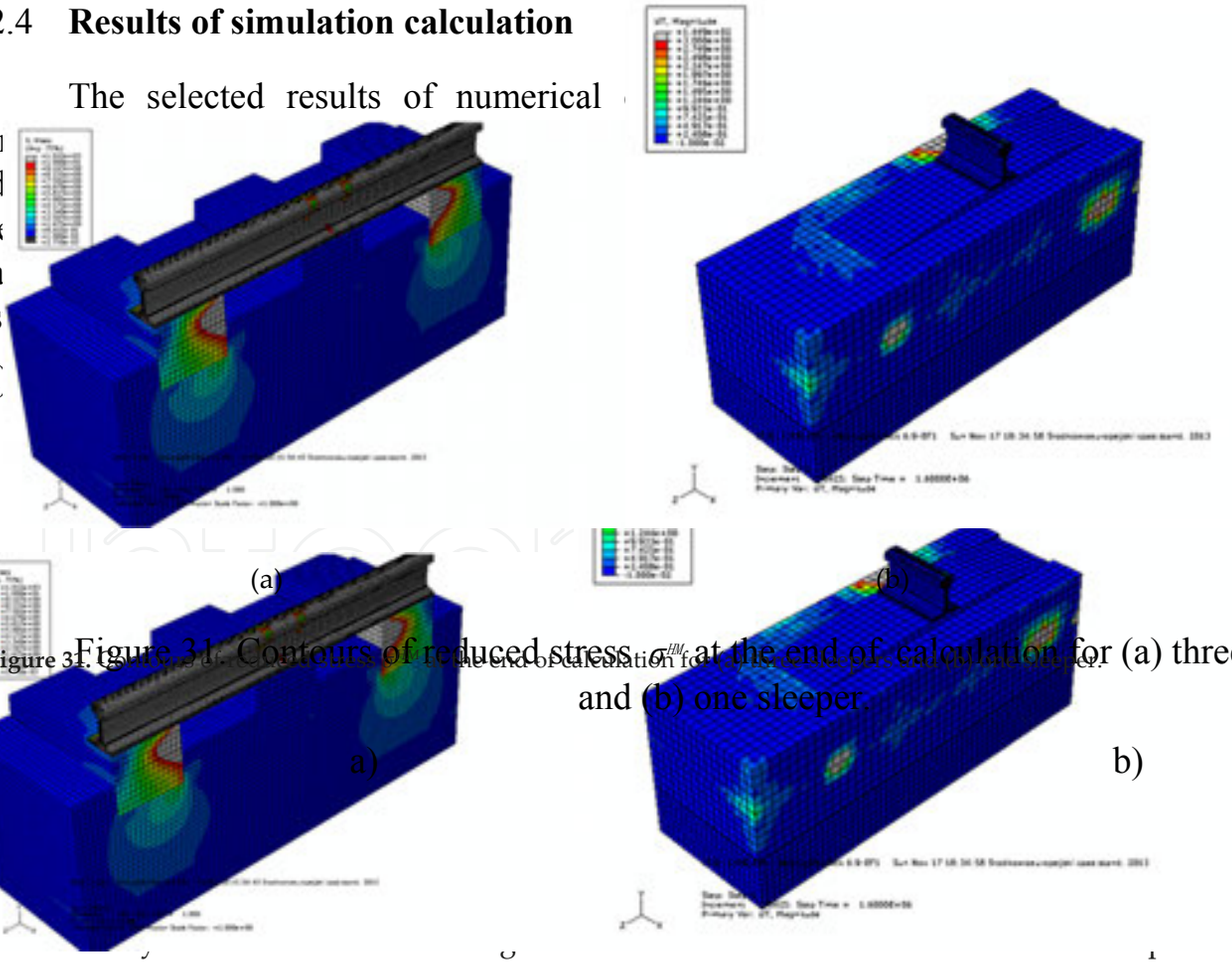

(a) (b)

Figure 31. Contours of reduced stress σ_{HM} at the end of calculation for (a) three sleepers and (b) one sleeper.

Figure 31. Contours of reduced stress σ_{HM} at the end of calculation for (a) three sleepers and (b) one sleeper.

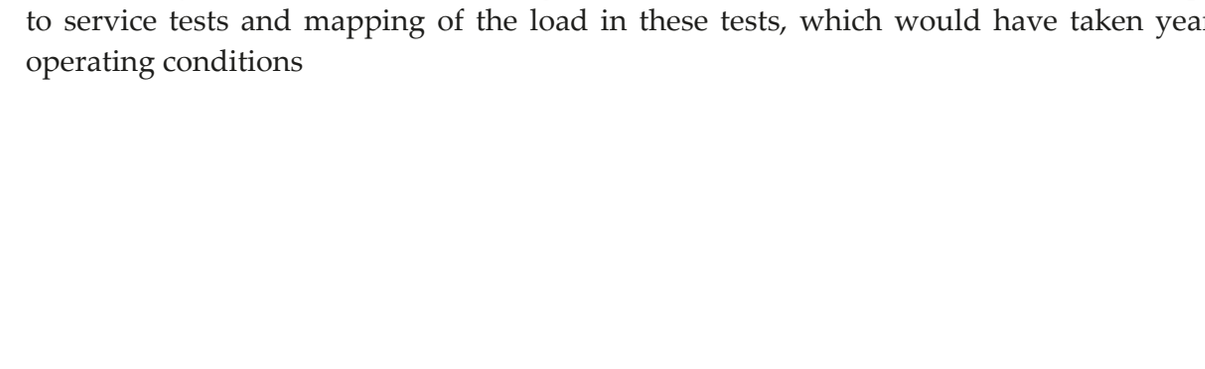

a) b)

to service tests and mapping of the load in these tests, which would have taken years in operating conditions

Figure 31. Contours of reduced stress σ^{HM} at the end of calculation for (a) three sleepers and (b) one sleeper.

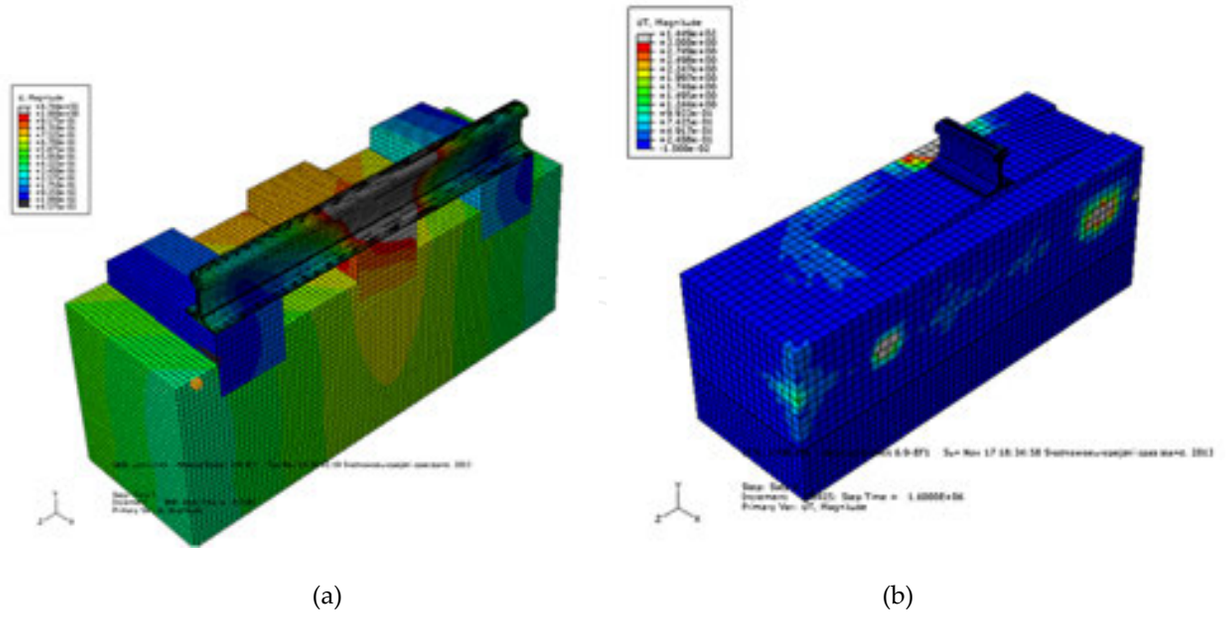

(a) (b)

Figure 32. Contours of strain maps for (a) three sleepers and (b) one sleeper.

Figure 32. Contours of strain maps for (a) three sleepers and (b) one sleeper.

5. Duration of guaranteed functionality

The duration of guaranteed functionality is a graphic representation of a fatigue performance of any railway track component as a function of operating load. At the initial operational stage, a slope of a strain accumulation curve for railway track structure is close to 90° and results from the railway track stabilization (subsidence). The next stage includes operation under load until the slope of a strain accumulation curve aims to reach higher values. Based on the simulation results obtained by the author of this chapter, as well as test results [22], the author have attempted to plot the curves describing the service life of selected railway track components. Figure 33 shows test results and simulation results contributing to the plastic strain relation as a function of operating load.

The graph shows a comparison of plastic strain vs. load at the testing track section, with or without railway track reinforcement using a geogrid and a resin. A curve plotted using simulation calculations is also included, although due to a long calculation time, the simulation curve is limited to 18 Tg load. The determination of a strain accumulation curve slope requires further tests and analyses to increase the operating load and continue observations.

6. Development and testing of superstructure

The track superstructure as a basic element of the railway system is crucial to the operation and safe management of the railway traffic. Changes in operating conditions of the railway, i.e., increased operational speeds of passenger trains up to 350 km/h or increased operational speeds of freight trains as well as increased permissible load up to 250 kN, result in higher

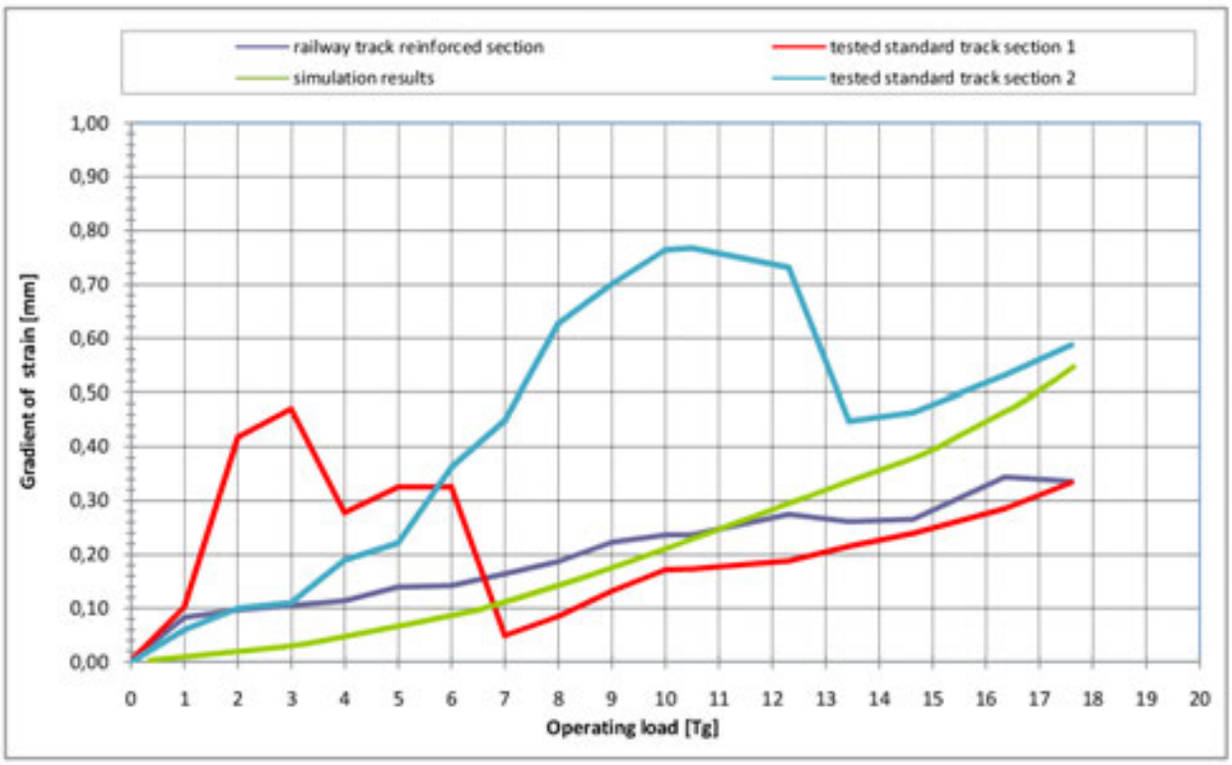

Figure 33. Theoretical model of duration of guaranteed functionality.

requirements for the track superstructures. The changes result in higher forces and vibration levels exerted on the superstructure. In addition, the economic aspects will force the designers and infrastructure operators to optimize the maintenance costs. A need to reduce the costs is one of the causes of using non-standard superstructures for high-speed rail networks. High operational speeds result in high ballast wear due to increased friction between the crashed stones. Increased wear requires more frequent ballast make up or replacement. Both standard requirements and technical specifications for interoperability (TSIs) guidelines for environmental protection, e.g., level of noise and vibrations are also key factors in improving track superstructure.

A question can be asked, if at the passenger train speeds over 350 km/h, is it reasonable to use standard ballast superstructure or use ballast-free solutions? More and more often, new solutions utilizing different materials used in the road engineering are also implemented in the railway solutions, including geomesh, geotextile, and various polyurethane resins, which may increase strength and durability of superstructures. It is also advisable to continue tests on fatigue effects at the rail/wheel interface and interactions between those surfaces. Incorrect mating between the railway vehicle and the rail may result in defects and damage to the running surface. Incorrect mating between the rail and the wheel may result from wheel polygonization and use of high-power trains, where incorrect wheel sidle protection (WSP) system is to prevent incorrect braking and starting. In high-speed trains, apart from basic braking system, also cleaning brake inserts are used to remove fouling from the running surfaces of wheels and railway track rails on which the trains travel.

http://dx.doi.org/10.5772/61517

7. Conclusions

The data presented in this section are a result of experimental and simulation tests performed by the author during 10 years of the research and scientific career. The discussed issues are a subject of interest for both manufacturers and experts responsible for the condition of a track superstructure. The stresses may affect the internal energy state of the material, phase changes, and corrosion of the material, reduce fatigue strength, and cause damage to the rails. The stresses are also one of the causes of accelerated development of standard railhead defects. The presented method of residual stresses evaluation using ultrasonic testing and numerical analysis in the course of the production process provides control over size and distribution of internal stresses due to bending and hardening processes. Another area of interest was related with the track superstructure tests, in particular involved seeking design solutions to reduce the maintenance costs by extending the time between repairs of the track superstructure components. The optimization of the maintenance costs by using advanced solutions in the track superstructure design may be an interesting method to extend its durability. The presented test results are the inspiration to continue the research in this area and seek new solutions, e.g., optimizing maintenance costs of the railway infrastructure, and determining structure durability using simulations.

Author details

Jacek Kukulski*

Address all correspondence to: jkukul@wt.pw.edu.pl

Faculty of Transport, Warsaw University of Technology, Warsaw, Poland

References

[1] Bałuch H. The concept of expert systems in the diagnosis of the superstructure and substructure. Problemy Kolejnictwa, 1996, 121 (in Polish).

[2] Bałuch M. Durability of the track ballast, 2008, 54(3), pp. 459–475.

[3] ORE D 182 Unified Assessment Criteria for Ballast Quality and Methods for Assessing the Ballast Condition in the Track. Report No. 3. Determining the Criteria for Ballast Durability Using Triaxial Tests, Utrecht, 1994.

[4] The dynamics of the mechanical system rail vehicle—track. Edited by J. Kisilowskiego. PWN, Warszawa, 1991 (in Polish).

[5] Szcześniak W. Selected Aspects of Rail—Interactions in a Vehicle–Railway Track–Substructure–Subsoil. Prace naukowe Budownictwo z. 129. Warszawa, 1995r. (in Polish).

[6] Bogdański S, Olzak M, Stupnicki J. Numerical stress analysis of rail rolling contact fatigue cracks. Optics and Lasers in Engineering 27, 1997, pp. 89–100.

[7] Liu Y, Liu L, Mahadevan S. Analysis of subsurface crack propagation under rolling contact loading in railroad wheels using FEM. Engineering Fracture Mechanics, 2007, 74, pp. 2659–2674. DOI: 10.1016/j.engfracmech.2007.02.012

[8] Kaewunruen S, Remennikov AM. Dynamic flexural influence on a railway concrete sleeper in track system due to a single wheel impact. Engineering Failure Analysis, 2008, 16(3), pp. 705–712.

[9] Kaewunruen S, Remennikov AM. Nonlinear Finite Element Modelling Of Railway Prestressed Concrete Sleeper. The Tenth East Asia-Pacific Conference on Structural Engineering and Construction, August 3–5, 2005, Bankok, Thailand, Vol. 4, pp. 323–328.

[10] Kaewunruen S, Remennikov AM. Impact capacity of railway prestressed concrete sleepers. Engineering Failure Analysis, 2008, 16(5), pp. 1520–1532.

[11] ElSawwaf MA. Behavior of strip footing on geogrid-reinforced sand over a soft clay slope. Geotextiles and Geomembranes, February 2007, 25(1), pp. 50–60.

[12] Dong Y-L, Han J, Bai X-H. Numerical analysis of tensile behavior of geogrids with rectangular and triangular apertures. Geotextiles and Geomembranes, April 2011, 29(2), pp. 83–91.

[13] Kukulski J. Selected numerical calculations for reinforced track substructure at various static and dynamic loads. Proceedings of the First International Conference on Railway Technology: Research, Development and Maintenance, Civil-Comp Press, Stirlingshire, UK. DOI: 10.4203/ccp.98.146. 2012, Paper 146. ISBN 978-1-905088-52-2.

[14] Kukulski J. Distribution of residual stresses of railway superstructure steel components after the rolling processes. Przegląd Komunikacyjny 2011, z. 9–10, ISSN: 0033-22-32. Pages: 74–77 (in Polish).

[15] Kukulski J. Evaluation of residual stresses condition in components of railway surface. Conference Rail Vehicles. Kazimierz Dolny 2006 (in Polish).

[16] Leykauf G, Lechner B, Stahl W. Improved ballasted track for high- speed lines. "Rail Engineering," London, 2004.

[17] D 71 ORE: Beanspruchung des Gleises, der Bettung und des Unterbaus durch Verkehrslasten. Beanspruchung der Bettung und des Unterbaus, Utrecht,1969, 72.

[18] Esveld C. Law maintenance ballastless track structures. Rail Engineering International Edition, 1997, 3.

[19] Fendrich L. Feste Fahrbahn Stadtbahn Berlin. Feste Fahrbahn. Edition ETR, Hestra Verlag, 1997.

[20] Adamski M. "Residual stresses." Materials Engineering. Warsaw, 1999 (in Polish).

[21] Radomski R. The residual stresses condition in rails. Materiały XX Jubileuszowej Konferencji Naukowej Komitetu Inżynierii Lądowej i Wodnej PAN. Kraków-Krynica, 1974 (in Polish).

[22] Basiewicz T, Towpik K, Gołaszewski A, Kukulski J. Evaluation of the accumulation of the irregularity in the experimental section of the track superstructure with composite ballast. Zeszyty Naukowo-Techniczne SITK RP o. w Krakowie No. 2(101)/2013 ISSN 1231–9171, pp. 19–27 (in Polish).

[23] Kukulski J. numerical calculations for track substructure—preliminary determination of durability of service life. In J. Pombo (editor), Proceedings of the Second International Conference on Railway Technology: Research, Development and Maintenance, Ajaccio-Corsica-France 8-11.04.2014, Railways 2014. Civil-Comp Press, Edinburgh, UK, 2014. DOI:10.4203/ccp.104.205, ISBN 978-1-905088-59.

IntechOpen